

**Serveur Académique Lausannois SERVAL [serval.unil.ch](http://serval.unil.ch)**

## **Author Manuscript**

### **Faculty of Biology and Medicine Publication**

**This paper has been peer-reviewed but does not include the final publisher proof-corrections or journal pagination.**

Published in final edited form as:

**Title:** Roles of mGluR5 in synaptic function and plasticity of the mouse thalamocortical pathway.

**Authors:** She WC, Quairiaux C, Albright MJ, Wang YC, Sanchez DE, Chang PS, Welker E, Lu HC

**Journal:** The European journal of neuroscience

**Year:** 2009 Apr

**Volume:** 29

**Issue:** 7

**Pages:** 1379-96

**DOI:** 10.1111/j.1460-9568.2009.06696.x

In the absence of a copyright statement, users should assume that standard copyright protection applies, unless the article contains an explicit statement to the contrary. In case of doubt, contact the journal publisher to verify the copyright status of an article.

Published in final edited form as:

*Eur J Neurosci.* 2009 April ; 29(7): 1379–1396. doi:10.1111/j.1460-9568.2009.06696.x.

## Roles of mGluR5 in synaptic function and plasticity of the mouse thalamocortical pathway

Wei-Chi She<sup>1</sup>, Charles Quairiaux<sup>3</sup>, Michael J. Albright<sup>1</sup>, Yu-Chi Wang<sup>1</sup>, Denisse E. Sanchez<sup>1</sup>, Poh-Shing Chang<sup>1</sup>, Egbert Welker<sup>3</sup>, and Hui-Chen Lu<sup>1,2</sup>

<sup>1</sup>The Cain Foundation Laboratories, Department of Pediatrics, Baylor College of Medicine, Houston, TX 77030 <sup>2</sup>Department of Neuroscience and Program in Developmental Biology, Baylor College of Medicine, Houston, TX 77030 <sup>3</sup>Département de Biologie Cellulaire et de Morphologie, Université de Lausanne, Lausanne, Switzerland

### Abstract

The group I metabotropic glutamate receptor 5 (mGluR5) has been implicated in the development of cortical sensory maps. However its precise roles in the synaptic function and plasticity of thalamocortical connections remain unknown. Here we first show that in mGluR5 knockout mice bred onto a C57BL/6 background cyto-architectonic differentiation into barrels is missing, but the representations for large whiskers are identifiable as clusters of thalamocortical afferents. The altered dendritic morphology of cortical layer IV spiny stellate neurons in mGluR5 knockout mice implicates a role for mGluR5 in the dendritic morphogenesis of excitatory neurons. Next, *in vivo* single unit recordings of whisker evoked activity in mGluR5 knockout adults demonstrated a preserved topographical organization of the whisker representation, but a significantly diminished temporal discrimination of center to surround whiskers in the responses of individual neurons. To evaluate synaptic function at thalamocortical synapses in mGluR5 knockout mice, whole-cell voltage clamp recording was conducted in acute thalamocortical brain slices prepared from postnatal day 4–11 mice. At mGluR5 knockout thalamocortical synapses, NMDA currents decayed faster and synaptic strength was more easily reduced, but more difficult to strengthen by Hebbian-type pairing protocols, despite a normal developmental increase in AMPAR-mediated currents and presynaptic function. We have therefore demonstrated that mGluR5 is required for synaptic function/plasticity at thalamocortical synapses as barrels are forming and we propose that these functional alterations at the thalamocortical synapse are the basis of the abnormal anatomical and functional development of the somatosensory cortex in the mGluR5 knockout mouse.

### Keywords

somatosensory cortex; mGluR; barrels; cortical maps; thalamocortical synapses

### Introduction

Cortical maps are composed of organized arrays of thalamocortical afferents projecting into distinct neuronal modules in cortical layer IV (Buonomano & Merzenich, 1998; Feldman & Brecht, 2005; Fox & Wong, 2005; Hensch, 2005). The mouse primary somatosensory (S1)

cortex is characterized by a row-and-arc pattern of “barrels”, replicating the arrangement of facial whiskers (Woolsey & Van der Loos, 1970; Killackey & Leshin, 1975). Neurons within single barrels respond to sensory input from their primary whiskers with a one-to-one relationship (Welker, 1976; Simons & Woolsey, 1979). Hebbian-based synaptic learning rules to adjust synaptic strength have been proposed to be the underlying mechanism for the formation and plasticity of cortical maps (Crair, 1999; Erzurumlu & Kind, 2001).

Thalamocortical (TC) connections are glutamatergic (Crair & Malenka, 1995; Kidd & Isaac, 1999). The critical period to induce Hebbian-type synaptic plasticity coincides with barrel formation (Crair & Malenka, 1995; Lu et al., 2001). Several aspects of synaptic function and plasticity at TC synapses are developmentally regulated, including an increase in the contribution of AMPARs, a change in NMDAR subunit composition from 2B- to 2A-dominant, and an acceleration of NMDA current decay kinetics (Agmon & O'Dowd, 1992; Barth & Malenka, 2001; Lu et al., 2001; Daw et al., 2007). Furthermore, the regulation of synaptic AMPARs and the formation of long-term potentiation are impaired in many mutant mice with defective barrel structures (Lu et al., 2003; Golshani et al., 2005; Inan et al., 2006; Lu et al., 2006). These findings indicate a central role for glutamate-mediated synaptic transmission in organizing the anatomical arrangements of TC pathways.

mGluR5, a group I metabotropic glutamate receptor (mGluR), has a prominent role in synaptic plasticity at many synapses (reviewed in Conn & Pin, 1997; Doherty & Dingledine, 2003; Collingridge et al., 2004; Kim et al., 2007). mGluR5 primarily activates Gαq/11, which stimulates phospholipase C (PLC) to generate the second messengers, inositol 1,4,5-trisphosphate (IP3) and diacylglycerol (DAG). These cumulative actions modulate various kinases, ion channels, and IP3-gated intracellular calcium stores. mGluR5 is expressed in the whisker-barrel pathway, including brainstem, thalamus, and cortex (Blue et al., 1997; Munoz et al., 1999; Lopez-Bendito et al., 2002) and its role in cortical barrel map development has been suggested by Hannan et al. (2001). mGluR5 is present in the postsynaptic compartments of developing TC synapses (Takasaki et al., 2008; Wijetunge et al., 2008). However, it is unclear how mGluR5 is involved in the functional development of TC pathways and how perturbation of mGluR5 signaling impacts sensory perception.

In this study we aimed to characterize the roles of mGluR5 in the dendritic morphogenesis and synaptic function/plasticity of TC synapses as barrels are forming, as well as in sensory processing in the adult using mGluR5 loss-of-function mutant mice. Specifically, several aspects of synaptic function and plasticity at TC synapses were analyzed using whole-cell patch-clamp recordings with acute TC brain slices, while *in vivo* single unit recording was conducted to explore sensory function. Together, our results indicate multiple roles for mGluR5 in the establishment and functioning of TC connections.

## Materials and Methods

### Animals and genotyping

mGluR5 mice in C57BL/6J background (B6.129-Grm5<sup>tm1Rod/J</sup>, stock number: 003558) were obtained from Jackson Laboratories (Bar Harbor, Maine) and were bred in a mGluR5<sup>+/-</sup> and mGluR5<sup>-/-</sup> mating strategy to produce mGluR5<sup>+/-</sup> and mGluR5<sup>-/-</sup> mice. mGluR5<sup>+/-</sup> littermates were used as controls. In preliminary experiments, breeding pairs of mGluR5<sup>+/-</sup> mice were set up to acquire mGluR5<sup>+/+</sup>, mGluR5<sup>+/-</sup>, and mGluR5<sup>-/-</sup> pups from the same litter and no difference between mGluR5<sup>+/+</sup> and mGluR5<sup>+/-</sup> were found for any of the studies conducted. In addition to the numbers of mGluR5<sup>+/-</sup> and mGluR5<sup>-/-</sup> animals used in this study mentioned throughout the Results, several mGluR5<sup>+/+</sup> mice were also used to examine cortical barrels with CO- and Nissl staining (n=7). All experiments and data analysis were done blinded to genotype. For genotyping, tail lysates were prepared by immersing tail pieces in 50 mM

NaOH, boiling for 30 minutes, vortexing vigorously for 10 sec, and then neutralizing with 1M Tris-HCl (pH8.0). Tail lysates were then vortexed for another 10 sec and centrifuged at 16,100 g for 1 minute. The supernatants were used as DNA templates for polymerase chain reaction (PCR) reactions. PCR reactions were conducted with a mixture of primers WT1 and WT2, Neo1 and Neo2. The PCR products of the first primer mix were 442 bp for the wt mGluR5 allele and 280 bp for the neo allele. The primer sequences were: WT1: 5'-CAC ATG CCA GGT GAC ATC AT -3'; WT2: 5'-CCA TGC TGG TTG CAG AGT AA -3'; Neo1: 5'-CTT GGG TGG AGA GGC TAT TC CC-3'; Neo2: 5'-AGG TGA GAT GAC AGG AGA TC -3'. Animals were treated in compliance with the U.S. Department of Health and Human Services and approved by Baylor College of Medicine. The animal handling procedures used for this study were also approved by the Office Veterinarian Cantonal (Lausanne) in accordance with Swiss Federal Laws.

### Tissue preparation

Mice were deeply anesthetized by an injection (3 ml/kg) of an anesthetic cocktail containing ketamine 37.6 mg/ml, xylazine 1.92 mg/ml and acepromazine 0.38 mg/ml. Following establishment of anesthesia, mice were transcardially perfused with ice-cold phosphate buffered saline (PBS), pH 7.4, followed by freshly prepared fixative (4% paraformaldehyde in PBS, PFA, pH 7.4). The brains were then post-fixed with the same fixative overnight at 4° C.

### Histology

The cytochrome oxidase (CO) and Nissl staining of brain sections were conducted as described (Lu *et al.*, 2001). Briefly, a fixed brain or flattened cortices (age range from P7 to P52) were sectioned to 100 or 50 µm thickness with a Leica VT-1000 Vibratome (Leica Microsystems, Bannockburn, IL) and placed in phosphate-buffered saline (PBS). For CO staining, 100 µm tangential slices were placed in CO reaction solution (5 mg diaminobenzidine, 5 mg cytochrome C, 0.4 g sucrose in 10 ml PBS, pH 7.4) for 1–18 hours at room temperature or 37° C. After staining, slices were rinsed with PBS and cover-slipped for imaging. For Nissl staining, serial 50 µm thick tangential sections were mounted on Superfrost-plus slides (Fisher Scientific, Hampton, NH). After drying, the entire series of sections throughout the cortical depth were stained with cresyl violet solutions. Sections were rinsed, dehydrated in graded alcohols to xylene, and then cover-slipped with xylene-based mounting medium (Cytoseal, Richard-Allen Scientific, Kalamazoo, MI).

### Antibodies

Primary antibodies (source and dilutions): mouse NeuN monoclonal Ab (Chemicon, 1:1000); rabbit anti-VGluT2 (vesicular glutamate transporter 2) polyclonal Ab (Synaptic System, Germany, 1:750). Secondary antibodies (and dilutions): goat anti-rabbit IgG-Alexa 488 (Molecular Probes, 1:1000); goat anti-mouse IgG-Cy3 (Jackson ImmunoResearch Laboratories, Pennsylvania, 1:500).

### Double immunofluorescent staining

Fixed brains were sectioned into 100 µm thick sections in tangential planes as described (Lu *et al.*, 2001). These tissue sections stayed free-floating for all subsequent steps. Sections were washed with PBST (PBS with 0.01% Triton X-100) and permeabilized with 0.2% Triton X-100 in PBS at room temperature for 20 minutes. Sections were then washed with PBST, blocked for one hour with 3% normal goat serum in PBST at room temperature, and then incubated with a mixture of two primary antibodies from different species in PBST with 2 mg/ml BSA and 1% normal goat serum at 4°C overnight. The next day, sections were washed with PBST, and incubated with the appropriate fluorescent secondary antibodies in PBST at room

temperature for two hours. Following this incubation, sections were washed with PBST three times for 10 minutes each. After DAPI staining (Molecular Probes, 1:3000 in PBS) to identify nuclei, sections were mounted onto Superfrost Plus slides, cover-slipped with PBS, and sealed with nail polish for confocal imaging.

## Imaging

24-bit RGB digital bright field images for histology were captured from an Olympus BX51 upright microscope with 2X, NA 0.08 objective under consistent light conditions using an Olympus DP70 CCD camera with Olympus DPC controller software. Confocal images were obtained using Olympus Fluo View FV300 software and an Olympus BX50WIF confocal microscope using 10X (NA, 0.4), 20X oil (NA, 0.8), or 60X oil (NA, 1.4) objectives. Alexa 488, and Cy3 fluorescence were excited with lasers of appropriate excitation wavelengths (488 nm and 543 nm) and scanned with the emission filters for maximum separation of the fluorophores (510/530 band pass filter for Alexa 488; 560/600 band pass filter for Cy3). Each image was acquired with the laser intensity adjusted to prevent over-saturation. All images were processed in Adobe Photoshop CS2 (San Jose, California) for brightness/contrast, orientation, and background correction to better illustrate the staining patterns. Regions of interest in digital images were copied and assembled into montages with Adobe Illustrator (San Jose, California).

## DiOlistic (gene gun) method

DiOlistic method was first described by Gan et al. (2000) and detailed protocols can be found in <http://wonglab.biostr.washington.edu/protocols.htm>. Briefly, animals were perfused with 4%PFA in PBS. The brains were then transferred to PBS and sectioned at 200  $\mu\text{m}$  with a Leica Vibratome in the thalamocortical plane. Sections containing the barrel field were stained with a CO-staining solution for one hour at room temperature. A gene gun was loaded with bullets prepared from 100 to 200 mg tungsten particles (Bio-Rad Laboratories, Hercules, California) coated with a mixture of DiI, DiO, and DiD (Molecular Probes). The Helio Gene Gun system (Bio-Rad) was used to make the bullets and deliver the labeled bullets to fixed brain slices (pressure, 80–120 psi). CO-stained slices were placed onto glass slides and the excess liquid was removed. The opening of gene gun was placed slightly off center of the barrel cortex so only a few neurons were labeled. After shooting, slices were mounted and examined with confocal microscopy the same day. Neurons were labeled by this method within a few minutes. Labeled spiny stellate neurons within the barrel field (distinguished by CO staining) were identified and imaged with confocal microscopy with 20X, 60X, or 100X objectives. Spiny stellate neurons were identified by the following criteria: (1) round-shape cell body, (2) a cell body diameter < 15  $\mu\text{m}$ , and (3) spiny dendrites.

The Neurolucida (Microbrightfield, Inc.) program was used to reconstruct the neurons or dendritic segments in three dimensions with confocal image stacks. Once the neuron was traced, Neuroexplorer (Microbrightfield, Inc.) divided the traced neurons into a series of dendritic segments and measured the length and angle of each segment. A polar histogram was generated by collecting the dendritic segments into 10-degree-wide bins according to segment angle from 0 to 360 degrees and plotted with the total length of dendritic segments in a given bin. Dendritic asymmetry ratios were then calculated from the polar histograms by dividing the sum of the lengths of the greatest continuous 180 degrees (18 neighboring bins) by the total length of all dendritic segments. This produces a ratio from 0.5 (perfectly symmetric) to 1 (extremely asymmetric, occurring only if all the dendritic segments for a particular neuron all point in the same direction plus or minus 5 degrees!). We defined neurons as asymmetric if they had asymmetry ratios greater than 0.75, indicating that the neuron had 75% of its dendritic segments pointing one direction.

### **In vivo single unit recordings**

A total of 17 adult female mice were used (weight 15–25g, between postnatal days 50 and 90). 52 neurons were recorded in 8 mGluR5<sup>+/-</sup> mice and 46 neurons in 9 mGluR5<sup>-/-</sup> mice, in the barrels C1, C2 and D2. Of these, 78 neurons were recorded in the C2-barrel: 50 in the mGluR5<sup>+/-</sup> and 28 in the mGluR5<sup>-/-</sup> group.

**Electrophysiological recordings**—Recordings were made under urethane anaesthesia (10% solution in distilled water; 2 mg/g body weight, i.p.) as described (Welker *et al.*, 1993; Quairiaux *et al.*, 2007). The mice were mounted in a stereotaxic frame (Narishige, Japan) equipped with a home-made head holder and a craniotomy of the right parietal bone was realized with a high speed dental drill to expose the somatosensory cortex. The exposed region was covered with 1% agar dissolved in 0.9% saline. Body temperature and depth of the anaesthesia were continuously monitored as previously described (Welker *et al.*, 1993; Quairiaux *et al.*, 2007). Extracellular neuronal activity was recorded using carbon fibre microelectrodes of low impedance (1–5 M $\Omega$ ; Armstrong-James & Millar, 1979; Armstrong-James *et al.*, 1980). The microelectrode was lowered into the cortex perpendicular to the pial surface using a three-dimensional micro drive and a reference electrode was placed at the level of the scalp. The differential voltage signal was recorded using a Neurolog modules arrangement (Neurolog system, Digitimer Ltd, UK), amplified (2000 times), then band-pass filtered (0.8–5 kHz). Single units were isolated and digitized by means of a waveform time window discriminator that (DIS-1, BAK electronic INC.). Digitized spike times were processed using the CED-Power 1401 interface (Cambridge Electronic Design, UK). Recording sites were targeted to layer IV, i.e. 350–480  $\mu$ m from pial surface (Welker *et al.*, 1993). Three neurons separated by a minimal distance of 50  $\mu$ m along the track were recorded during a single microelectrode penetration. One to three penetrations in barrel column C2, C1 and/or D2 were achieved in each animal, separated tangentially by a minimal distance of 100  $\mu$ m. Evoked responses of barrel column neurons were all recorded towards their PW and 6 to 8 immediate surround whiskers, one at a time. The whisker stimulus consisted of an upward deflection of 1.43° from the horizontal plane of 3 ms duration, applied with a piezoelectric bimorph slab. Each individual whisker was deflected 50 times, at a frequency of 0.5 Hz. During the recording session, the principal whisker (PW) was defined as the whisker that evoked responses at the shortest latency. Following each recording session, the correspondence between PWs and recording sites were histologically verified using microlesions. Penetrations were marked at the end of each session by electrolytic lesions (1.6  $\mu$ A negative current during 7 seconds; see Welker *et al.*, 1993) made 400  $\mu$ m from pial surface and CO-stained sections were processed in order to visualize the position of the microlesions with respect to the barrel outlines.

**Data analysis**—Spike times were collected into 1 ms bins in two separate channels, retrieving either all spike times following each whisker deflection to build peristimulus time histograms (PSTHs) or only the time of the first spike after stimulus onset (defined as latency) to build latency histograms (LHs) and analysed using Spike 2 software (Cambridge Electronic Design, UK). The response magnitude (RM) of a single unit was defined as the mean number of spikes per stimulus evoked between 3 and 100 ms after the stimulus onset and corrected for the spontaneous activity, determined from the pre-stimulus 100 ms spike count. Based on the LHs, median latencies and interquartile ranges (IQR) were calculated with a precision of 1 ms.

**Statistics**—The distributions of RM and latencies to individual whiskers were tested for normality (Shapiro-Wilk test). Normality was rejected in half of the cases; data were therefore normalized with a transform ranking method before entering a multivariate hierarchical model (“group animal (group)”; GLM procedure). The hypothesis of no overall group effect on the cluster of dependant variables, i.e. RM or latencies to PW and SWs, was tested with a

multivariate analysis of variance (MANOVA) test criteria (Wilk's lambda). Where the null hypothesis was rejected, multiple comparisons of each variable between groups could then be performed with minimized risks of false positive (Type II error) using Tukey's studentized range HSD (honestly significant difference) tests, which included inter-animal variability as a potential error source. All statistics were realized with SAS package for windows (SAS Institute Inc., USA).

### ***In vitro* electrophysiology and data analysis**

Acute thalamocortical brain slices were prepared from P4-P10 (day of birth is P0) mouse pups as described (Lu et al., 2001). Slices were maintained and recorded at room temperature in artificial cerebral spinal fluid (ACSF; compositions in mM: 124 NaCl, 5 KCl, 1.25 NaH<sub>2</sub>PO<sub>4</sub>, 1.3 MgSO<sub>4</sub>, 2 CaCl<sub>2</sub>, 26 NaHCO<sub>3</sub>, and 11 glucose) saturated with 95% O<sub>2</sub> and 5% CO<sub>2</sub>. The whole-cell internal solution contained the following (in mM): 117.5 cesium gluconate, 17.5 CsCl, 8 NaCl, 10 HEPES, 0.2 EGTA, 4 Mg-ATP, 0.3 GTP, and 7 phosphocreatine, pH 7.2, 290–300 mOsm. 10 mM BAPTA was included in the whole-cell internal solution to prevent inadvertent potentiation of the postsynaptic neuron when NMDAR-mediated currents were measured and LTD experiments conducted.

Field potentials and voltage-clamped excitatory postsynaptic currents (EPSCs) were recorded from layer IV neurons in S1 of P6-8 mice using a Multiclamp 700B amplifier (Axon instruments). For field potential recordings, the recording electrode was filled with ACSF and stimulation strength of 0–200  $\mu$ A at 25  $\mu$ A intervals with a Neurolog NL800A stimulus isolator (Digitimer, Ltd.) was applied to ventrobasal thalamus through bipolar sharpened tungsten microelectrodes (Frederick Haer Company, Bowdoinham, ME). The nonspecific glutamate receptor antagonist kynurenic acid (10 mM; Sigma) was routinely added to the perfusate at the end of the recordings to ensure the correct identification of fiber volley and synaptic response. Fiber volley amplitudes and the slopes of field excitatory postsynaptic potential (fEPSP) were calculated from averages of 20 sweeps at each stimulus intensity.

For whole-cell voltage-clamped recordings, cells were held at  $-70$  mV except where otherwise indicated. Stimuli (0.1 – 0.2 ms duration) were applied to the ventrobasal thalamus through a computer-triggered stimulus isolator (BAK Electronics, Inc.). Data were collected (10 kHz sampling rate with 2 KHz Bessel filter) using pClamp 9.2 (Molecular Devices, Sunnyvale, CA) and analyzed with Clampfit. To evaluate and monitor the health of the cell, input and series resistances were continuously monitored, and cells that had  $< 300$  M $\Omega$  input resistance or drifted  $> 20\%$  discarded. Only responses that exhibited short and constant latencies (5–10 ms) that did not change with increasing stimulus intensity were considered monosynaptic. Half-saturating stimulation strength with a relatively low stimulation frequency (10–30 s inter-stimulus intervals) was used to evoke stable EPSCs. More than ten minutes of baseline response was usually acquired prior to any treatments. EPSC amplitudes were calculated by subtracting the peak amplitude from the baseline taken from 2–3 ms before the stimulus. In our TC slice preparations, the areas responding to stimulations applied to VB tend to localize to the barrel field corresponding to small rostro-ventral whiskers and thus almost all the electrophysiological recordings were conducted in small barrels.

Long term potentiation (LTP) and depression (LTD) were induced using pairing protocols described previously (Lu et al., 2003). For LTP experiments, the inter-stimulus interval was 20–30 sec. Briefly, LTP pairing was initiated by switching to a holding potential of  $-10$  mV and stimulating with 100 Hz stimuli. The percentage of EPSC change was calculated as the mean EPSC amplitude of sweeps recorded at 21–30 min after pairing minus the mean EPSC amplitude of 20 sweeps acquired during baseline recordings (baseline amplitude) divided by the baseline amplitude. LTD was induced by depolarizing the postsynaptic cell to  $-40$  mV for

100 stimuli while the stimulation frequency remained at 0.1 Hz. The level of depression was determined using the same method as described above for LTP.

To measure the AMPA/NMDA current ratio, the cell was held at  $-70$  mV to measure AMPAR-mediated currents. To measure NMDA currents, the cell was depolarized to  $+40$  mV to relieve the  $Mg^{2+}$  block of the NMDAR, while  $10$   $\mu$ M NBQX and  $10$   $\mu$ M Gabazine were added to the perfusate to block AMPA, kainate, and GABA-A receptors (Lu et al., 2001). Cesium ions in the whole-cell solution blocked GABA<sub>B</sub>-activated K channel responses. The AMPA/NMDA current ratios, the ifenprodil sensitivities and percentage of EPSC changes triggered by pairings were quantified from the average of 20 consecutive EPSCs.

The decay kinetics of the NMDAR-mediated currents were determined by fitting a double exponential function ( $A_1e^{-t/\tau_1} + A_2e^{-t/\tau_2}$ ) to the first 800 ms of the decaying phase of the current of the average trace derived from 10–20 sweeps. The value of the weighted time constant was defined as  $\tau_{\text{weighted}} = \tau_1 \times A_1/(A_1 + A_2) + \tau_2 \times A_2/(A_1 + A_2)$ . Ifenprodil-insensitive NMDA currents were obtained by bath application of  $3$   $\mu$ M ifenprodil in addition of NBQX and Gabazine for 20–30 min while holding the cell at  $+40$  mV. The ifenprodil sensitivity was defined as the percentage of ifenprodil-sensitive current to total NMDAR-mediated current. NBQX, Gabazine, ifenprodil were from Tocris Bioscience (Ellisville, MO). To measure evoked mini, stable whole-cell voltage-clamp recordings were established at a  $-70$  mV holding potential, and the  $Ca^{2+}$  in the ACSF was exchanged for  $Sr^{2+}$ -ACSF ( $3$  mM  $Sr^{2+}$ , containing  $10$   $\mu$ M Gabazine and  $50$   $\mu$ M D-AP5 (D-(-)-2-amino-5 phosphopentanoic acid (Tocris Bioscience) to eliminate inhibitory currents and possible NMDAR current contamination, respectively. Evoked AMPA-mEPSCs were recorded in one sec epochs every two sec. Paired pulse responses of AMPAR-mediated currents were recorded by paired-stimuli with 50, 100, or 500 msec intervals. For MK801 experiments, NMDA current was isolated and only cells responding with a significant amount of NMDA current ( $> 15$  pA) were used. After acquiring a stable baseline response (15–20 minutes), the stimulation was stopped and ACSF containing (+)-MK801 ( $40$   $\mu$ M, Tocris) was perfused onto the slice ( $1$  ml/min flow rate). After 10 minutes (to allow enough time for MK801 to equilibrate in the recording chamber), we resumed stimulation and recorded until no NMDA current could be detected for more than 5 minutes. The time course of MK801-dependent blockade was analyzed by normalizing all of the responses to the amplitude of the first NMDA response after MK801 was applied.

All summary data are presented as means  $\pm$  standard error. Student's t-test was used to determine statistical significance except where otherwise specified.

## Results

### Abnormal sensory maps in mGluR5 loss-of-function mutant mice

The whisker representations in S1 consist of discrete clusters of thalamocortical afferents (TCAs) surrounded by the cell bodies of cortical layer IV neurons, the latter forming the sides of the barrels. To examine the formation of whisker representations in mGluR5 knockout (KO) mice in the C57BL6 background (back-crossed for more than seven generations; mGluR5<sup>-/-</sup>), histochemistry with cytochrome oxidase (CO) and Nissl staining and immunostaining with thalamocortical and neuronal markers were conducted (Fig. 1). Animals were bred using an mGluR5 heterozygous (mGluR5<sup>+/-</sup>) and homozygous (mGluR5<sup>-/-</sup>) mating strategy to produce mGluR5<sup>+/-</sup> and mGluR5<sup>-/-</sup> mice. mGluR5<sup>+/-</sup> littermates were used as controls. Histological sections were prepared from various ages in a plane tangential to the pial surface of the barrel cortex (P7–P52, day of birth is P0; the barrel pattern is similar between P7–P52 so the data from P7 and P16 are shown as examples). In contrast to the discrete CO pattern observed in all paired mGluR5<sup>+/-</sup> littermates (Fig. 1A,C;  $n = 21$ ), the boundaries of CO-stained patches corresponding to the small rostro-ventral whiskers were very indistinct in

mGluR5<sup>-/-</sup> mice, whereas those corresponding to the large caudo-dorsal whiskers were recognizable (Fig. 1B,D; n = 15). Discrete barrel rings of layer IV neurons were revealed by Nissl-staining in mGluR5<sup>+/-</sup> mice (Fig. 1E, n = 8). However, no clear cytoarchitectural differentiation of layer IV neurons into barrels was detected in mGluR5<sup>-/-</sup> mice, whereas a few vaguely visible patches of Nissl-staining (reflecting clusters of cell bodies) were observed at the level of the representation of the most caudo-dorsal whiskers (Fig. 1F; n = 7).

Vesicular glutamate transporter protein 2 (VGluT2) is a reliable marker for TCAs (Fujiyama *et al.*, 2001; Hur & Zaborszky, 2005; Nahmani & Erisir, 2005). Thus, the segregation of TCAs in the S1 cortex of mGluR5<sup>-/-</sup> mice was also examined by immunostaining with antibodies against VGluT2 (Fig. 1G–J). At P7, the cortical whisker map deficit in mGluR5<sup>-/-</sup> mice (n = 3) detected by VGluT2 immunostaining (Fig. 1H) in tangential sections was similar to the pattern observed with CO-staining (Fig. 1B). Double labeling of VGluT2 and NeuN were used to reveal simultaneously the distributions of TCAs and layer IV neurons in the representation of the small rostro-ventral whiskers (Fig. 1I,J). Complementary matches between TCA clusters and barrels (formed by the ring-like arrangement of the cell bodies of layer IV neurons) were detected in mGluR5<sup>+/-</sup> mice (n = 2) but no clear relationship between the distributions of TCAs and layer IV neuronal cell bodies was found in mGluR5<sup>-/-</sup> mice (n = 3). Taken together, these results show that at the level of the representation of the small rostro-ventral whiskers both the segregation of TCA and the cytoarchitectonic differentiation into barrels are disrupted in mGluR5<sup>-/-</sup> mice, whereas at the level of the representation of the large caudo-dorsal whiskers TCAs segregate into individual whisker-representations, without the cytoarchitectonic differentiation into barrels. These data point to a crucial role of mGluR5 in the cellular differentiation of cortical layer IV neurons in S1 cortex that are post-synaptic to TCA input.

### Dendritic morphology of layer IV neurons is altered in mGluR5 KO mice

Most layer IV neurons have their cell bodies in the side of the barrel and send their dendrites toward the barrel hollow where they form synapses with clusters of TCAs receiving inputs from individual whiskers (Woolsey *et al.*, 1975; Steffen & Van der Loos, 1980; Lubke *et al.*, 2000; Datwani *et al.*, 2002). The asymmetrical orientation of dendrites to match pre-synaptic partners is likely guided by activity-dependent processes (Erzurumlu & Kind, 2001; Inan & Crair, 2007). The absence of barrel patterns in mGluR5 KO mice may result from an alteration of dendritic morphogenesis. To examine dendritic morphogenesis of layer IV spiny stellate neurons, the DiOlistic method (Gan *et al.*, 2000) was used to label neurons in mGluR5<sup>+/-</sup> or mGluR5<sup>-/-</sup> mice at various ages. Layer IV spiny neurons in the representation of the large postero-caudal whiskers were imaged with confocal microscopy. Their structures were reconstructed in three dimensions and analyzed with the NeuroLucida program (Fig. 2). Most mGluR5<sup>-/-</sup> stellate neurons had rather symmetrical distributions of their dendrites, in contrast to the polarized distribution of the dendrites of control neurons (Fig. 2A–F). The dendritic asymmetry (defined in Materials and Methods) of mGluR5<sup>-/-</sup> neurons was significantly reduced in both juveniles (2–3 weeks old; mGluR5<sup>+/-</sup>,  $0.81 \pm 0.03$ , 15 neurons from five animals; mGluR5<sup>-/-</sup>,  $0.69 \pm 0.02$ , 20 neurons from five animals;  $p = 0.003$ ) and adults (4–7 weeks old; mGluR5<sup>+/-</sup>,  $0.75 \pm 0.02$ , 20 neurons from four animals; mGluR5<sup>-/-</sup>,  $0.68 \pm 0.02$ , 20 neurons from five animals;  $p = 0.048$ ; Fig. 2G). In mGluR5<sup>+/-</sup> mice, 64% neurons showed an orientation bias, while only 27% mGluR5<sup>-/-</sup> neurons had a polarized distribution of their dendrites (neurons with a dendritic asymmetry value greater than 0.75 were considered to be polarized; Fig. 2J). The dendritic span (the longest distance of the dendritic tips) was significantly larger in mGluR5<sup>-/-</sup> neurons (mGluR5<sup>+/-</sup> juveniles,  $218.25 \pm 17.00 \mu\text{m}$ , 16 neurons from six animals; mGluR5<sup>-/-</sup> juveniles,  $275.13 \pm 16.58 \mu\text{m}$ , 23 neurons from six animals;  $p = 0.018$ , Mann-Whitney *U* Test; mGluR5<sup>+/-</sup> adults,  $205.76 \pm 11.44 \mu\text{m}$ , n = 20 neurons from four animals; mGluR5<sup>-/-</sup> adults,  $288.24 \pm 17.09 \mu\text{m}$ , n = 20 neurons from five animals;  $p < 0.001$ ; Fig. 2H). Interestingly, mGluR5<sup>-/-</sup> neurons had more dendritic segments

than mGluR5<sup>+/-</sup> neurons (mGluR5<sup>+/-</sup>, 24.08 ± 1.89 segments, n = 36 neurons from nine animals; mGluR5<sup>-/-</sup>, 28.98 ± 1.83 segments, n = 43 neurons from ten animals; p = 0.048, Mann-Whitney U Test; Fig. 2I). In summary, the dendritic morphology of layer IV mGluR5<sup>-/-</sup> neurons was perturbed in both orientation and outgrowth.

### Deficient spatial segregation of whisker input to layer IV neurons in mGluR5<sup>-/-</sup> mice

In the adult barrel cortex, neurons located in single barrels receive sensory input predominantly from individual whiskers (Welker, 1976; Simons & Woolsey, 1979; Armstrong-James & Fox, 1987; Welker *et al.*, 1993). To examine the receptive field characteristics in S1 of mGluR5<sup>-/-</sup> mice, *in vivo* single-unit physiological recordings were conducted to quantify the response properties of layer IV neurons to whisker deflections. The principal whisker (PW) was defined as the whisker that evoked responses at the shortest latency and had a strong response magnitude (RM). The magnitude and latency of single-unit responses to activation of PW and surround whiskers (SWs) were recorded (Fig. 3). All neurons (52 neurons from eight mGluR5<sup>+/-</sup> mice and 46 neurons from nine mGluR5<sup>-/-</sup> mice) responded significantly to the deflection of PW and SWs. The activation of the PW elicited a maximal RM in 51/52 neurons in mGluR5<sup>+/-</sup> mice and 44/46 neurons in mGluR5<sup>-/-</sup> mice. The RM to the PW was significantly stronger than the RM of any SWs in both genotypes (at p < 0.001; multivariate non parametric statistics and Kruskal-Wallis). There was a slight but insignificant decrease in the RM to PW deflections in mGluR5<sup>-/-</sup> mice (mGluR5<sup>+/-</sup>, 1.24 ± 0.07 spikes, n = 52; mGluR5<sup>-/-</sup>, 1.08 ± 0.06 spikes, n = 47; p = 0.15; Fig. 3B). The latency of responses to the PW was not different between the two strains (median latencies and IQR: mGluR5<sup>+/-</sup>, 12.5 ms and 11.0 to 18.7 ms; mGluR5<sup>-/-</sup>, 15 ms and 12.0 to 20.0 ms; p = 0.71; Fig. 3C).

Nearly all cells encountered during a single penetration respond preferentially to the same SW with the strongest RM and fastest latency compared to any other SW within their receptive field as described previously (Armstrong-James *et al.*, 1992; Welker *et al.*, 1993; Petersen & Diamond, 2000). In other words, there is a dominant SW within the surround receptive field. Interestingly, in mGluR5<sup>-/-</sup> mice, several neurons responded to the dominant SW with a very short latency. Some of them even responded at similar latency as the PW. In contrast, all neurons showed a substantial delay between the latency to the PW and the fastest SW in mGluR5<sup>+/-</sup> mice. In accordance with this observation, the distributions of median latency differences between responses to the PW and the dominant SW were quite different between mGluR5<sup>+/-</sup> and mGluR5<sup>-/-</sup> mice (Fig. 3D). In mGluR5<sup>+/-</sup> mice, only 4 % of neurons show a latency delay ≤ 5ms. However, in the mGluR5<sup>-/-</sup> mice, the proportion of neurons responding to the dominant SW with a delay ≤ 5ms increased to more than 20%. The mean difference in latency to the PW and the dominant SW was significantly shorter in the mGluR5<sup>-/-</sup> mice (mean and sem: 13.47 ± 2.29 sec, n = 36) than in the mGluR5<sup>+/-</sup> mice (23.48 ± 2.29 sec, n = 45; p = 0.005, non parametric Mann-Whitney U test; Fig. 3E). A similar decrease in the latency of the dominant SW has also been reported in *barrelless* mice (Welker *et al.*, 1996). The neurons showing the shortest delays between the PW and the dominant SW were also characterized by strong RMs (mGluR5<sup>+/-</sup>, 0.41 ± 0.05 spikes, n = 48; mGluR5<sup>-/-</sup>, 0.47 ± 0.05 spikes, n = 42; p = 0.19). However, the relative RM from the dominant SW to the PW was not different between mGluR5<sup>+/-</sup> and mGluR5<sup>-/-</sup> mice. In sum, these *in vivo* recordings of whisker evoked activity in mGluR5 knockout adults demonstrated a significantly diminished temporal discrimination of center to surround whiskers in the response of individual mGluR5<sup>-/-</sup> neurons.

### Altered synaptic plasticity in mGluR5 KO TC synapses

Activity-dependent processes have been proposed to coordinate the development of the pre-(TCAs) and post-synaptic components (layer IV neurons) of barrels. Such mis-matched whisker patterns in mGluR5 KO S1 cortex suggests the involvement of mGluR5 mediated synaptic transmission in organizing layer IV neurons according to the TCA-pattern. The

neurotransmission at TC synapses is mainly mediated by AMPA ( $\alpha$ -amino-3-hydroxy-5-methyl-4-isoxazolepropionate), kainate, and NMDA (N-methyl-D-aspartate) receptors (Crair & Malenka, 1995; Kidd & Isaac, 1999). Long-term potentiation (LTP) and depression (LTD) at TC synapses can only be induced during the first postnatal week (Crair & Malenka, 1995; Isaac *et al.*, 1997; Feldman *et al.*, 1998; Lu *et al.*, 2001). It has been proposed that Hebbian-type synaptic plasticity is the cellular mechanism underlying activity-dependent processes in neural circuit formation (Crair, 1999; Erzurumlu & Kind, 2001). We and others have explored the activity-dependent mechanisms underlying cortical map development with various mutant mice having defective barrels, including *barrelless* (a spontaneous mutant mice with a loss of function mutation in the  $\text{Ca}^{2+}$ /calmodulin activated adenylyl cyclase type I gene, AC1), protein kinase A regulatory subunit II beta (PKARII $\beta$ ) KO, and forebrain-specific DNA methyltransferase 1 (Dnmt1) KO mice (Lu *et al.*, 2003; Golshani *et al.*, 2005; Inan *et al.*, 2006; Lu *et al.*, 2006). Both LTP and LTD are difficult to induce in *barrelless* TC synapses (Lu *et al.*, 2003). In PKARII $\beta$  and Dnmt1 KO mice, LTP is also defective (Golshani *et al.*, 2005; Inan *et al.*, 2006). mGluR5 has a role in synaptic plasticity at many synapses (for examples see: Lu *et al.*, 1997; Jia *et al.*, 1998; Huber *et al.*, 2001; Sung *et al.*, 2001; Gubellini *et al.*, 2003; Puyal *et al.*, 2003; Bender *et al.*, 2006b; Harney *et al.*, 2006; Nevian & Sakmann, 2006; Neyman & Manahan-Vaughan, 2008). But its role in regulating the functional properties of TC synapses has not been examined. We hypothesized that some aspects of TC synaptic plasticity depend on mGluR5 function and that these deficits may cause the whisker-pattern abnormalities in mGluR5<sup>-/-</sup> mice.

To examine the general features of synaptic transmission in mGluR5<sup>-/-</sup> TC synapses, we first analyzed the input-output relationships of synaptic responses from a large population of layer IV neurons in acute TC slices prepared from mGluR5<sup>-/-</sup> and their littermate controls using field potential recordings with a range of stimulus intensities (0–200  $\mu\text{A}$  at 25  $\mu\text{A}$  intervals). Typical fEPSP responses in layer IV of barrel cortex triggered by thalamic stimulation are composed of a short latency fiber volley and a longer latency synaptic response (Agmon & Connors, 1991; Fig. 4). The initial slope of the fEPSP gives a good estimate of the monosynaptic response, while the fiber volley amplitude reflects the number of TCAs stimulated. Gradual increases in the fiber volley amplitudes and fEPSP slopes were observed when the stimulation intensity was raised (Fig. 4A). Indistinguishable input-output relationships were found when comparing the slopes of fEPSPs to the amplitudes of the fiber volley between P6–8 mGluR5<sup>+/-</sup> (n = 6) and mGluR5<sup>-/-</sup> (n = 7) mice. These data indicate that synaptic transmission is grossly normal from TCAs onto S1 layer IV neurons in mGluR5<sup>-/-</sup> mice (Fig. 4B).

Next, whole-cell voltage clamp recordings were conducted to examine LTP formation at mGluR5<sup>+/-</sup> and mGluR5<sup>-/-</sup> TC synapses. A standard LTP pairing protocol (Crair & Malenka, 1995) was used to induce LTP at P4–6 TC synapses, the age when robust LTP can be induced in wild type mice (Lu *et al.*, 2001). Substantial long-lasting increases in AMPAR-mediated currents after pairing were observed in six out of seven mGluR5<sup>+/-</sup> cells recorded (Fig. 5). Interestingly, the same LTP pairing protocol induced depression or only a slight potentiation at mGluR5<sup>-/-</sup> TC synapses. The percentage of excitatory postsynaptic current (EPSC) change 21–30 minutes after LTP pairing at mGluR5<sup>-/-</sup> TC synapses was significantly smaller than the change induced in their littermate controls (mGluR5<sup>+/-</sup>,  $81.6 \pm 32.9\%$ , n = 7; mGluR5<sup>-/-</sup>,  $3.2 \pm 11.5\%$ , n = 9; p = 0.026). These data provides strong evidence to support a role of mGluR5 in TC-LTP formation.

Several studies with pharmacological blockers have found that acute blockade of mGluR5 function prevent LTD formation (Huber *et al.*, 2001; Sung *et al.*, 2001; Puyal *et al.*, 2003; Bender *et al.*, 2006a; Nevian & Sakmann, 2006). To explore if the absence of mGluR5 will prevent TC-LTD formation, experiments with a standard LTD-pairing protocol were

conducted in P4-6 mGluR5<sup>+/-</sup> and mGluR5<sup>-/-</sup> cells (Fig. 5). Unexpectedly, the degree of synaptic depression triggered was significantly stronger at mGluR5<sup>-/-</sup> TC synapses compared to control synapses (the percentage change of the EPSC 11–20 minutes after LTD pairing: mGluR5<sup>+/-</sup>,  $-0.36 \pm 6.64\%$ ,  $n = 7$ ; mGluR5<sup>-/-</sup>,  $-34.83 \pm 10.32\%$ ,  $n = 11$ ;  $p = 0.03$ , Mann-Whitney  $U$  test). These results indicate that the complete absence of mGluR5 in the KO mice alters postsynaptic physiology, which facilitates synaptic depression triggered by coordinated neural activity.

### Normal developmental increase of AMPARs at mGluR5 KO TC synapses

Several aspects of synaptic function at TC synapses are developmentally regulated, including an increase in the contribution of AMPARs, a change in NMDAR subunit composition from 2B- to 2A-dominant, and an acceleration of NMDA current decay kinetics (Agmon & O'Dowd, 1992; Barth & Malenka, 2001; Lu *et al.*, 2001; Daw *et al.*, 2007). During the first postnatal week, thalamic stimulation often evokes large NMDA EPSCs but relatively small AMPA EPSCs. After P7, the relative contribution from AMPARs increases significantly while those from NMDARs decrease. The functional maturation of AMPA currents in TC synapses is usually studied by analyzing the ratio of evoked AMPA/NMDA currents recorded from P7-9 layer IV neurons. Deficits in the developmental increase of AMPA/NMDA current ratios at TC synapses are present in many barrel-lacking mice, including *barrelless* mice, as well as PKARII $\beta$ , and Neuro-D2 KO mice (Lu *et al.*, 2003; Inan *et al.*, 2006; Ince-Dunn *et al.*, 2006). To explore the putative role of mGluR5 in the development of TC synapses, we recorded evoked AMPAR and NMDAR-mediated EPSCs from P7-P9 mGluR5<sup>+/-</sup> and mGluR5<sup>-/-</sup> layer IV neurons (Fig. 6A,B). Robust AMPA currents were recorded and the AMPA/NMDA current ratios at TC synapses were similar for both genotypes (mGluR5<sup>+/-</sup>,  $2.05 \pm 0.44$ ,  $n = 13$ ; mGluR5<sup>-/-</sup>,  $2.52 \pm 0.69$ ,  $n = 12$ ;  $p = 0.165$ , Mann-Whitney  $U$  Test).

An unchanged AMPA/NMDA ratio may simply reflect similar changes in both AMPA and NMDA currents when mGluR5 is absent. Thus potential AMPA current deficits can only be revealed when absolute AMPA currents are compared between control and mGluR5 KO cells. In the presence of Sr<sup>2+</sup>, neurotransmitter release at axon terminals is desynchronized and evoked miniature events are observed in response to quantal release at single synapses (Xu-Friedman & Regehr, 1999). Studies in *barrelless*, PKARII $\beta$  KO, and cortical-AC1 KO mice found that the amplitudes of AMPAR-mediated miniature events at single TC synapses were smaller than at wild type synapses (Lu *et al.*, 2003; Inan *et al.*, 2006; Iwasato *et al.*, 2008 Golshani, 2005 #326). To examine if there is a change in synaptic strength mediated by AMPARs at mGluR5 KO TC synapses, evoked AMPA miniature-EPSCs (evoked AMPA-mEPSCs) were examined by replacing Ca<sup>2+</sup> with Sr<sup>2+</sup> in the extracellular solution as described (Lu *et al.*, 2003). Briefly, stable and synchronized responses were established in regular Ca<sup>2+</sup>-containing extracellular solution (artificial cerebrospinal fluid, ACSF) and then Sr<sup>2+</sup>-ACSF was washed in. The substitution of Ca<sup>2+</sup> with Sr<sup>2+</sup> quickly led to a reduction in the amplitudes of synchronized EPSCs and the appearance of numerous asynchronous quantal events (Fig. 7A). The distribution of the amplitudes of evoked AMPA-mEPSCs was similar between mGluR5<sup>+/-</sup> and mGluR5<sup>-/-</sup> mice (Fig. 7B,C). No significant difference was found in the mean amplitudes (mGluR5<sup>+/-</sup>,  $15.60 \pm 2.04$  pA,  $n = 7$ ; mGluR5<sup>-/-</sup>,  $13.54 \pm 2.39$  pA,  $n = 6$ ;  $p = 0.52$ ; Fig. 7D) or kinetics of the evoked AMPA-mEPSCs from P6-P10 mGluR5<sup>+/-</sup> and mGluR5<sup>-/-</sup> TC synapses (for 10–90 % rise time: mGluR5<sup>+/-</sup>,  $1.60 \pm 0.17$  msec,  $n = 7$ ; mGluR5<sup>-/-</sup>,  $1.93 \pm 0.27$  msec,  $n = 6$ ;  $p = 0.32$ ; for 10–90 % decay time: mGluR5<sup>+/-</sup>,  $5.82 \pm 0.26$  msec,  $n = 7$ ; mGluR5<sup>-/-</sup>,  $6.52 \pm 0.41$  msec,  $n = 6$ ;  $p = 0.16$ ; Fig. 7E,F). These results, together with the normal AMPA/NMDA ratios found at mGluR5<sup>-/-</sup> synapses, suggest that mGluR5 is not required to regulate the developmental increase of AMPARs at TC synapses.

### Synaptic NMDAR's in mGluR5 KO TC synapses have fast-decay current kinetics

The kinetics of NMDAR-mediated currents evolve from slow-decaying to fast-decaying currents around the end of the first postnatal week and these changes parallel the switch of NMDAR subunit composition from NR2B- to NR2A-dominant forms (Barth & Malenka, 2001; Lu *et al.*, 2001). In NR2A KO TC synapses, the decay kinetics of NMDAR currents are much slower than at NR2A-wild type synapses after the first postnatal week (Lu *et al.*, 2001). Interestingly, here we found that NMDA currents measured at P7-9 in mGluR5<sup>-/-</sup> TC synapses (Fig. 6C; the weighted time constant:  $145.9 \pm 6.4$  msec,  $n = 9$ ) decayed significantly faster than at control synapses (the weighted time constant:  $201.3 \pm 54.2$  msec,  $n = 13$ ;  $p = 0.008$ ). To probe if this change in current kinetics is caused by a change in NMDAR subunit composition, the sensitivity of NMDA currents to ifenprodil were analyzed (Fig. 6D,E). Ifenprodil is an NR2B-specific antagonist and the percentage of NMDA current blocked by ifenprodil can be used to estimate the relative contributions of NR2B-containing NMDAR's. Ifenprodil sensitivity was slightly, but non-significantly reduced in mGluR5<sup>-/-</sup> TC synapses (mGluR5<sup>+/-</sup>,  $34.00 \pm 6.86\%$ ,  $n = 9$ ; mGluR5<sup>-/-</sup>,  $25.90 \pm 4.22\%$ ,  $n = 12$ ;  $p = 0.303$ ). In other words, ifenprodil block did not uncover any obvious differences in the NMDAR composition of mGluR5<sup>-/-</sup> TC synapses.

### Normal presynaptic function at mGluR5 KO TC synapses

To gain insight into whether mGluR5 loss-of-function results in presynaptic functional deficits, two electrophysiology paradigms were conducted to examine the short-term plasticity and neurotransmitter release probabilities at mGluR5<sup>-/-</sup> TCAs. We first used a paired-pulse protocol to characterize the short term plasticity of TC synapses in P7-P10 mGluR5 KO and control neurons (Fig. 8). Paired-pulse ratios (PP ratios) were determined by measuring the ratio of the amplitude of the second response to the first response from two closely spaced stimuli. PP ratios are typically inversely correlated with the probability of neurotransmitter release (Pr) and are a standard measure of presynaptic function (Zucker & Regehr, 2002). We measured the responses of TC synapses evoked with paired stimuli of three different inter-stimulus intervals (ISIs), 50, 100, and 500 msec (abbreviated as PP50, PP100, or PP500 for the following). In both control and mGluR5 KO cells, paired stimuli produced strong paired-pulse depression, consistent with previous findings (Gil *et al.*, 1999; Yanagisawa *et al.*, 2004) and no difference in the PP ratios of AMPA currents ( $p$  values:  $p = 0.724$  for PP50,  $p = 0.949$  for PP100;  $p = 0.928$  for PP500) was found between mGluR5<sup>+/-</sup> (the ratios: PP50,  $0.86 \pm 0.15$ ,  $n = 10$ ; PP100,  $0.80 \pm 0.29$ ,  $n = 9$ ; PP500,  $0.58 \pm 0.21$ ;  $n = 9$ ) and mGluR5<sup>-/-</sup> TC synapses (the ratios: PP50,  $0.75 \pm 0.27$ ,  $n = 6$ ; PP100,  $0.70 \pm 0.38$ ,  $n = 8$ ; PP500,  $0.55 \pm 0.19$ ;  $n = 7$ ). Thus, short-term plasticity of TC synapses is unaffected by the mGluR5 loss-of-function mutation.

MK801 is an irreversible NMDAR open channel blocker. Measuring the rate at which NMDA currents are blocked by MK801 during repetitive stimulation provides an indirect method to estimate the probability of release (Hessler *et al.*, 1993; Rosenmund *et al.*, 1993; Manabe & Nicoll, 1994). This method depends on the fact that NMDA receptors must first be opened before they can be blocked by MK801, and the blockade is essentially irreversible. NMDA-EPSC amplitudes decrease progressively with repeated stimuli in the presence of MK801, and the rate of NMDA channel blockade varies inversely with the probability of vesicular release. We found that the decay of NMDA currents by MK801 blockade occurred very rapidly in P7-10 mGluR5<sup>+/-</sup> and mGluR5<sup>-/-</sup> cells (Fig. 9). The inhibition kinetics by MK801 was estimated by fitting the decay of the NMDA-EPSC in MK801 for each cell by single exponential and no difference was found between two genotypes (mGluR5<sup>+/-</sup> tau:  $9.15 \pm 0.97$  stimuli,  $n = 12$ ; mGluR5<sup>-/-</sup> tau:  $11.87 \pm 1.92$  stimuli,  $n = 6$ ;  $p = 0.18$ ). This finding indicates that the release efficacy at mGluR5<sup>-/-</sup> TCAs is normal.

Taken together, these studies with various *in vitro* electrophysiological paradigms show that the absence of mGluR5 alters NMDAR function and the direction of synaptic plasticity but

doesn't affect AMPAR functional maturation or the development of presynaptic release machinery at TC synapses.

## Discussion

In mGluR5 KO mice, the organization of layer IV neurons and whisker-related TCA clusters are “mismatched” with complete absence of the architectonic organization of layer IV neurons while the large whisker-related TCA clusters remain. The symmetrical dendritic morphogenesis of layer IV spiny stellate neurons in these mice may account for the non-segregated positioning of their cell bodies and the diminished temporal discrimination of principal to surround whiskers in the responses of individual adult S1 layer IV neurons revealed by *in vivo* single unit recordings of whisker evoked activity. However, the topographical organization of the whisker representation is preserved in mGluR5 KO mice. At developing mGluR5 KO TC synapses, the kinetics of NMDAR-mediated currents and the formation of synaptic plasticity at TC synapses are both altered. However, both the developmental increase in AMPAR-mediated currents and presynaptic function are normal in the TC synapses of mGluR5 KO mice. Taken together, these results show that mGluR5 signaling plays a central role in the formation of cortical maps, the synaptic maturation of TC synapses, and sensory processing.

### The role of mGluR5 at thalamocortical synapses

mGluR5 modulates various kinases, ion channels, and IP<sub>3</sub>-gated intracellular calcium stores through DAG and IP<sub>3</sub> signaling and has a prominent role in synaptic plasticity at many synapses (reviewed in Conn & Pin, 1997; Doherty & Dingledine, 2003; Collingridge *et al.*, 2004; Kenny & Markou, 2004; Kim *et al.*, 2007). Recently, it has been found that mGluR5 is present in the postsynaptic compartments of developing TC synapses (Takasaki *et al.*, 2008; Wijetunge *et al.*, 2008). Here we showed that mGluR5 regulates various aspects of synaptic function and plasticity at TC synapses. At mGluR5 KO TC synapses, LTP formation is defective while LTD is enhanced. Thus, the absence of mGluR5 transforms TC synapses into a state that is prone to depression by coordinated neural activity. It has been proposed that Hebbian-type synaptic plasticity depends on the characteristics of calcium influx (Gall *et al.*, 2005). It is likely that the amount and duration of the calcium increase determines the signaling cascades triggered, which in turn determines the direction of synaptic plasticity (Holcman *et al.*, 2005). The fast-decaying NMDA current kinetics at mGluR5 KO synapses are likely to allow less calcium influx when NMDARs are triggered by neural activity. Since mGluR5 couples to IP<sub>3</sub>-gated intracellular calcium stores, the calcium rise derived from internal stores triggered by neural activity is likely to be less in mGluR5 KO synapses (Conn & Pin, 1997; Doherty & Dingledine, 2003; Collingridge *et al.*, 2004; Kenny & Markou, 2004; Kim *et al.*, 2007). We propose that the reduced amount of calcium signaling triggered by neural activity in mGluR5 KO synapses prevents LTP formation.

The LTP deficit observed here at mGluR5 KO TC synapses is consistent with previous findings in hippocampus CA1 (Lu *et al.*, 1997; Jia *et al.*, 1998). However, our studies found that the consequences of genetic deletion of mGluR5 are different from pharmacological blockade of this receptor in several aspects. Studies using pharmacological blockers (e.g. the mGluR5-specific antagonist MPEP) typically find that acute blockade of mGluR5 receptors prevents LTD formation (Huber *et al.*, 2001; Sung *et al.*, 2001; Puyal *et al.*, 2003; Bender *et al.*, 2006b; Nevian & Sakmann, 2006). At wild type TC synapses, pairing-induced LTD formation can also be blocked by MPEP treatment (data not shown). Surprisingly, the degree of synaptic depression triggered by the same pairing paradigm was significantly stronger in mGluR5 KO TC synapses compared to control synapses. This is unlikely to be caused by the compensatory up-regulation of other mGluRs as the expression of other mGluRs is normal in mGluR5 KO

mice (Lu *et al.*, 1997). Acute blockade of mGluR5 with MPEP slowed NMDA current kinetics (data not shown), the opposite of what was observed in mGluR5 KO TC synapses. Thus, the acute blockade of mGluR5 using a pharmacological antagonist affects synaptic function of TC synapses differently compared to the complete absence of mGluR5. One plausible explanation for this discrepancy is that the absence of mGluR5 changes the composition of the postsynaptic densities. Such alteration may allow synaptic depression to be more easily triggered by coordinated neural activity.

The developmental increase in AMPAR-mediated currents has been observed in various synapses (reviewed in (Malinow & Malenka, 2002; Song & Huganir, 2002)). NMDAR-dependent TC LTP formation leads to an increase in AMPA currents and un-silencing of silent synapses (Crair & Malenka, 1995; Isaac *et al.*, 1995; Feldman *et al.*, 1999). It has been proposed that an endogenous LTP-like process is the underlying mechanism for the developmental increase in AMPA currents at TC synapses (Inan & Crair, 2007). Our studies in mGluR5 KO mice challenge this dogma. Despite the defective LTP and enhanced LTD formation, the AMPA/NMDA current ratios and the amplitudes of evoked AMPA-mEPSC's in mature TC synapses are normal in mGluR5 KO mice. Growing evidence points to the presence of NMDAR-independent mechanism to regulate the synaptic insertion of AMPARs at nascent synapses (Groc *et al.*, 2006; Hall & Ghosh, 2008). For example, a substantial AMPA current was detected in S1 cortex of Cx-NR1 KO mice (Iwasato *et al.*, 2000). Taken together, while LTP- and LTD-like mechanisms can modulate synaptic strength by regulating AMPAR trafficking, a different mechanism is used to increase synaptic AMPARs at nascent synapses.

There is a gradual increase in the NR2A contribution to NMDAR currents in TC synapses during the first postnatal week that parallels the change in the NMDA current kinetics from slow to fast (Lu *et al.*, 2001). NMDAR kinetics remain slow in NR2A KO TC synapses. A role for calcineurin in modulating NMDA current kinetics in the superior colliculus has been proposed (Shi *et al.*, 2000). It remains to be determined if calcineurin modulates NMDA kinetics in TC synapses. The faster NMDA kinetics in mGluR5 KO mice could be explained by a reduced NR2B contribution in NMDAR. However, only a slight and insignificant difference in the NR2A/2B ratio was detected comparing mGluR5 KO and control synapses using the NR2B-specific antagonist, ifenprodil. The caveat of this paradigm is that ifenprodil will block NMDARs with any number of NR2B subunits. Wijetunge *et al.* (2008) found a reduced NR2B expression in mGluR5 KO mice on a mixed C57BL6/129 background. Thus, the faster kinetics of NMDARs in mGluR5 KO TC synapses may result from a reduced number of NR2B in heteromeric synaptic NMDARs.

### **mGluR5 and NMDARs collaborate at thalamocortical synapses**

There is extensive evidence supporting crosstalk between NMDAR and mGluR5 signaling. Proteomic and biochemical analysis found that mGluR5 and NMDARs are present in the same protein complex and interact through Homer, Shank, and PSD-95 (postsynaptic density-95; Fagni *et al.*, 2004). The absence of mGluR5 leads to an impairment in the tetanus-induced potentiation of NMDAR-mediated responses in CA1 pyramidal neurons (Lu *et al.*, 1997). The activation of type I mGluRs leads to tyrosine phosphorylation of NR2A/B subunits and the enhancement of NMDA currents (Heidinger *et al.*, 2002; Guo *et al.*, 2004) and the absence of mGluR5 leads to a reduction of NMDA currents in CA1 pyramidal neurons (Lu *et al.*, 1997). Harney *et al.* (2006) found that mGluR5 determines the directionality of synaptic plasticity of NMDA receptor-mediated synaptic transmission. Interestingly, depriving sensory information from all but one whisker (uni-vibrissa experience) triggers a change from a NMDAR- to mGluR-dependent mechanism for synaptic strengthening in layer II/III neurons of S1 cortex (Clem *et al.*, 2008).

The characteristics of the cortical whisker map deficit observed here in mGluR5 KO mice are very similar to those reported for cortex-specific NMDAR subunit 1 (Cx-NR1) KO mice (Iwasato *et al.*, 2000; Datwani *et al.*, 2002). In both mutant mice, the TCA clusters corresponding to small whiskers are almost absent, while a few TCA clusters representing large whiskers remain. Furthermore, in both mice there is no obvious pattern formed by the layer IV neurons, even in the areas where TCA clusters remain. Instead of sending their dendrites toward barrel hollows to synapse onto TCAs, mGluR5- and NR1-KO layer IV neurons project their dendrites into a wider area and fail to assume a particular orientation. The total number of spiny stellate neuron dendrites increases in both mutant mice, suggesting that both NMDAR and mGluR5 are required to prune or stop dendritogenesis. However, neither receptor seems to play a critical role for axonal path-finding or target recognition, since in both mutant mice TCAs reach their proper location and target correct cortical layers. Taken together, our data and prior results, respectively, suggest both mGluR5 and NMDAR are required to form “barrel” aggregates and to orchestrate the dendritic morphogenesis of layer IV neurons to match their presynaptic partners, the TCAs.

Here we found changes in both the kinetics of NMDAR-mediated currents and NMDAR-dependent LTP formation at mGluR5 KO TC synapses. It is plausible that KO of mGluR5 results in abnormal NMDAR function leading to a defective barrel pattern. However, it is equally possible that mGluR5 and NMDAR share signaling cascades to instruct barrel development and synaptic function/plasticity at TC synapses. Taken together, our data and prior results, respectively, suggest both mGluR5 and NMDAR interact at TC synapses and may work together to orchestrate the cytoarchitecture of layer IV neurons to match the TCAs.

### Distinct features differentiate *barrelless* and mGluR5 KO mice

*Barrelless* mice with the AC1 loss-of-function mutation were the first mutant mice with a barrel map deficit to be identified (Welker *et al.*, 1996). The anatomical and functional properties of TC connections, as well as sensory processing from whiskers-to-barrels have been characterized extensively in *barrelless* mice (Welker *et al.*, 1996; Abdel-Majid *et al.*, 1998; Lu *et al.*, 2003; Lu *et al.*, 2006). The anatomical characteristics of the cortical whisker map deficits in *barrelless* and mGluR5 KO mice have interesting differences. In *barrelless* S1 cortex, the whisker-related CO-patterns are completely absent with lack of segregation of TCA arborizations (Welker *et al.*, 1996; Abdel-Majid *et al.*, 1998; Gheorghita *et al.*, 2006). In mGluR5 KO mice, the architectonic organization of layer IV neurons is absent while the TCA clusters (as visualized with cytochrome oxidase histochemistry and VGLuT2 immunostaining) are present at the representation of the large caudo-dorsal whiskers.

Despite the abnormal morphology of the whisker representation in S1, *in vivo* single unit recordings demonstrated that both *barrelless* and mGluR5 KO mice have topographical representations for individual whiskers and that the cortical neurons respond to deflection of their principal whisker with short latency and maximal magnitude. However, the latency of the response to the dominant surround whisker from mGluR5 KO neurons was significantly faster than from control neurons. The short latency response, similar to those of the principal whisker, from the dominant surround whiskers was also observed in *barrelless* mice (Welker *et al.*, 1996). Because of their altered, non-segregated, positioning and their broad symmetrical dendritic projections, layer IV spiny stellate neurons of mGluR5 KO mice may receive direct inputs from thalamic afferents relaying sensory responses from neighboring whiskers, accounting for this short latency. The absence of AC1 in cortical neurons also leads to less polarized distributions of dendrites of layer IV neurons (Iwasato *et al.*, 2008). Taken together, the dendritic morphology of cortical layer IV neurons likely affects their sensory responses. However, other mechanisms may be involved in modifying the sensory response, like an alteration in the wiring of the intracortical, inhibitory circuits or that of recurrent excitatory

connections of layer IV neurons in mGluR5 KO. A detailed quantitative study on the intracortical axonal projection patterns of these two classes of neurons could be envisaged.

At the synaptic level, both LTP and LTD formation in TC synapses are defective in *barrelless* mice (Lu *et al.*, 2003). Interestingly, in mGluR5 KO TC synapses, LTP formation is absent while the degree of depression triggered by a LTD pairing paradigm is enhanced. Thus, the absence of mGluR5 at TC synapses leaves the synapse in a state that is prone to depression by coordinated neural activity, while AC1 is required for synaptic plasticity in both directions. Our previous work also found defective presynaptic function in *barrelless* TCAs. Here we found normal presynaptic properties at mGluR5 KO synapses. Normal presynaptic function of TC connections was also found in cortical-specific AC1 KO mice (Iwasato *et al.*, 2008). Taken together, these data suggest that AC1 in TCAs regulate neurotransmission directly and loss of mGluR5 does not alter neurotransmitter release. mGluR5 and AC1 are likely to regulate synaptic function and plasticity through different signaling cascades.

### Partial whisker maps in mGluR5 KO mice

The only vibrissa-related pattern remaining visible in mGluR5 KO mice is the representation of the large caudo-dorsal whiskers on the snout. Such partial whisker maps have also been observed in MAOA KO (Vitalis *et al.*, 2002), SynGAP KO (Barnett *et al.*, 2006), PKARII $\beta$  KO (Watson *et al.*, 2006), and cortex-specific NR1 KO mice (Iwasato *et al.*, 2000). Interestingly, none of the mutant mice with whisker map deficits have a partial map representing only the small rostro-ventral whiskers. What are the differences between the representations for large and small whiskers? Why do the patterns for small whiskers get so easily lost? During embryogenesis, there is a gradient by which the whisker pad develops: the first follicles appear at the “delta corner” where the straddle whiskers ( $\alpha, \beta, \gamma$ ) are located, the last ones develop at the rostral ends of rows A and B (Andres & Van der Loos, 1982; Van der Loos *et al.*, 1986). A similar progressive development of the TCA pattern from the postero-medial (large barrels) to antero-lateral side (small barrels) occurs for the barrel field (Andres & Van der Loos, 1982; Van der Loos *et al.*, 1986; Rebsam *et al.*, 2002). The size of the barrels in S1 cortex reflects the density of innervation with the same topological order as on the snout (Welker & Van der Loos, 1986a). In mice with extra whiskers, only the whiskers receiving substantial innervation form an extra barrel (Welker & Van der Loos, 1986b). One explanation for the formation of a partial whisker-map in mGluR5 KO mice is that mGluR5 is required for the neural-activity dependent processes underlying cortical map formation. With the loss of mGluR5 there is a reduction in the activity-driven signal from individual whiskers. In this model, the strength of signals from small whiskers, due to their sparse innervation, falls below the threshold for pattern formation. In contrast, because of their greater innervation, the signals from large whiskers exceed the critical threshold, even when the level of activity is reduced in the mGluR5 KO.

In comparison, Hannan *et al.* (2001) found that TCAs in mGluR5<sup>-/-</sup> mice with a mixed genetic background segregated into individual rows, but not individual barrels, whereas in our case segregation into individual barrels was present in the representation of the large, caudal whiskers. This difference indicates that the severity of barrel map deficits resulting from the absence of mGluR5 function is influenced by the genetic background. However, Wijetunge *et al.* (2008) using the same strain of mGluR5 KO mice as used in the studies of Hannan *et al.* (2001) reported the same TCA pattern phenotype as we observed here. Perhaps the relative genetic contribution of C57BL6 vs 129 in this C57BL6/129 line has shifted more towards the C57 phenotype. In other words, the row-like TCA pattern in mGluR5 KO mice originally reported can no longer be detected. Nevertheless, the cytoarchitectural differentiation of layer IV neurons into barrels is uniformly disrupted despite the variable degree of TCA segregation.

The current study provides the first demonstration of how mGluRs contribute to the functional development of TC synapses and instruct anatomical arrangements of cortical neurons. The comparisons of the receptive field properties in adult *barrelless* and mGluR5 KO mice allow us to dissociate the sensory deficits derived from the overly extensive TCA arborizations versus deformed architectonic organizations of layer IV neurons. Our data suggest that NMDAR and mGluR5 collaborate with each other in shaping the cortical circuit that underlies single whisker processing in the adult somatosensory cortex.

## Acknowledgements

We would like to thank Dr. Ken Mackie for helpful comments on the manuscript. This work is supported by: NIH grants NS048884 (HCL), and ES07332 (MJA); NARSAD (HCL) and Swiss NSF grant 310000-108246 (EW).

## Abbreviations

*ACI*, the Ca<sup>2+</sup>/calmodulin activated type I adenylyl cyclase gene  
 ACSF, artificial cerebral spinal fluid  
 C, caudal  
 cd, the representation of the caudo-rostral whiskers  
 CO, cytochrome oxidase  
 D, dorsal  
 DAG, diacylglycerol  
 EPSCs, excitatory postsynaptic currents  
 fEPSP, field excitatory postsynaptic potential  
 KO, knockout  
 IP3, inositol 1,4,5-trisphosphate  
 LTP, long-term potentiation  
 LTD, long-term depression  
 mEPSC, miniature-EPSCs  
 mGluRs, metabotropic glutamate receptors  
 mGluR5, metabotropic glutamate receptor 5  
 PBS, phosphate buffered saline  
 PBST, PBS with 0.01% Triton X-100  
 PCR, polymerase chain reaction  
 PFA, paraformaldehyde  
 PKARI $\beta$ , the protein kinase A regulatory subunit II beta  
 PLC, phospholipase C  
 PW, principal whisker  
 R, rostral  
 RM, response magnitude  
 rv, the representation of the rostro-ventral whiskers  
 S1, the primary somatosensory cortex  
 SW, surround whisker

## References

- Abdel-Majid RM, Leong WL, Schalkwyk LC, Smallman DS, Wong ST, Storm DR, Fine A, Dobson MJ, Guernsey DL, Neumann PE. Loss of adenylyl cyclase I activity disrupts patterning of mouse somatosensory cortex. *Nat Genet* 1998;19:289–291. [PubMed: 9662407]
- Agmon A, Connors BW. Thalamocortical responses of mouse somatosensory (barrel) cortex *in vitro*. *J Neurosci* 1991;41:365–379.
- Agmon A, O'Dowd DK. NMDA receptor-mediated currents are prominent in the thalamocortical synaptic response before maturation of inhibition. *J Neurophysiol* 1992;68:345–349. [PubMed: 1381421]

- Andres FL, Van der Loos H. Whisker patterns form in cultured non-innervated muzzle skin from mouse embryos. *Neurosci Lett* 1982;30:37–41. [PubMed: 7099496]
- Armstrong-James M, Fox K. Spatiotemporal convergence and divergence in the rat S1 "barrel" cortex. *J Comp Neurol* 1987;263:265–281. [PubMed: 3667981]
- Armstrong-James M, Fox K, Das-Gupta A. Flow of excitation within rat barrel cortex on striking a single vibrissa. *J Neurophysiol* 1992;68:1345–1358. [PubMed: 1432088]
- Armstrong-James M, Fox K, Millar J. A method for etching the tips of carbon fibre microelectrodes. *J Neurosci Methods* 1980;2:431–432. [PubMed: 7412368]
- Armstrong-James M, Millar J. Carbon fibre microelectrodes. *J Neurosci Methods* 1979;1:279–287. [PubMed: 544972]
- Barnett MW, Watson RF, Vitalis T, Porter K, Komiyama NH, Stoney PN, Gillingwater TH, Grant SG, Kind PC. Synaptic Ras GTPase activating protein regulates pattern formation in the trigeminal system of mice. *J Neurosci* 2006;26:1355–1365. [PubMed: 16452659]
- Barth AL, Malenka RC. NMDAR EPSC kinetics do not regulate the critical period for LTP at thalamocortical synapses. *Nat Neurosci* 2001;4:235–236. [PubMed: 11224537]
- Bender KJ, Allen CB, Bender VA, Feldman DE. Synaptic basis for whisker deprivation-induced synaptic depression in rat somatosensory cortex. *J Neurosci* 2006a;26:4155–4165. [PubMed: 16624936]
- Bender VA, Bender KJ, Brasier DJ, Feldman DE. Two coincidence detectors for spike timing-dependent plasticity in somatosensory cortex. *J Neurosci* 2006b;26:4166–4177. [PubMed: 16624937]
- Blue ME, Martin LJ, Brennan EM, Johnston MV. Ontogeny of non-NMDA glutamate receptors in rat barrel field cortex: I. Metabotropic receptors. *J Comp Neurol* 1997;386:16–28. [PubMed: 9303522]
- Buonomano DV, Merzenich MM. Cortical plasticity: from synapses to maps. *Annu Rev Neurosci* 1998;21:149–186. [PubMed: 9530495]
- Clem RL, Celikel T, Barth AL. Ongoing in vivo experience triggers synaptic metaplasticity in the neocortex. *Science* 2008;319:101–104. [PubMed: 18174444]
- Collingridge GL, Isaac JT, Wang YT. Receptor trafficking and synaptic plasticity. *Nat Rev Neurosci* 2004;5:952–962. [PubMed: 15550950]
- Conn PJ, Pin JP. Pharmacology and functions of metabotropic glutamate receptors. *Annu Rev Pharmacol Toxicol* 1997;37:205–237. [PubMed: 9131252]
- Crair MC. Neuronal activity during development: permissive or instructive? *Curr Opin Neurobiol* 1999;9:88–93. [PubMed: 10072369]
- Crair MC, Malenka RC. A critical period for long-term potentiation at thalamocortical synapses. *Nature* 1995;375:325–328. [PubMed: 7753197]
- Datwani A, Iwasato T, Itohara S, Erzurumlu RS. NMDA receptor-dependent pattern transfer from afferents to postsynaptic cells and dendritic differentiation in the barrel cortex. *Mol Cell Neurosci* 2002;21:477–492. [PubMed: 12498788]
- Daw MI, Scott HL, Isaac JT. Developmental synaptic plasticity at the thalamocortical input to barrel cortex: Mechanisms and roles. *Mol Cell Neurosci*. 2007
- Doherty J, Dingledine R. Functional interactions between cannabinoid and metabotropic glutamate receptors in the central nervous system. *Curr Opin Pharmacol* 2003;3:46–53. [PubMed: 12550741]
- Erzurumlu RS, Kind PC. Neural activity: sculptor of 'barrels' in the neocortex. *Trends Neurosci* 2001;24:589–595. [PubMed: 11576673]
- Fagni L, Ango F, Perroy J, Bockaert J. Identification and functional roles of metabotropic glutamate receptor-interacting proteins. *Semin Cell Dev Biol* 2004;15:289–298. [PubMed: 15125892]
- Feldman DE, Brecht M. Map plasticity in somatosensory cortex. *Science* 2005;310:810–815. [PubMed: 16272113]
- Feldman DE, Nicoll RA, Malenka RC. Synaptic plasticity at thalamocortical synapses in developing rat somatosensory cortex: LTP, LTD, and silent synapses. *J Neurobiol* 1999;41:92–101. [PubMed: 10504196]
- Feldman DE, Nicoll RA, Malenka RC, Isaac JT. Long-term depression at thalamocortical synapses in developing rat somatosensory cortex. *Neuron* 1998;21:347–357. [PubMed: 9728916]
- Fox K, Wong RO. A comparison of experience-dependent plasticity in the visual and somatosensory systems. *Neuron* 2005;48:465–477. [PubMed: 16269363]

- Fujiyama F, Furuta T, Kaneko T. Immunocytochemical localization of candidates for vesicular glutamate transporters in the rat cerebral cortex. *J Comp Neurol* 2001;435:379–387. [PubMed: 11406819]
- Gall D, Prestori F, Sola E, D'Errico A, Roussel C, Forti L, Rossi P, D'Angelo E. Intracellular calcium regulation by burst discharge determines bidirectional long-term synaptic plasticity at the cerebellum input stage. *J Neurosci* 2005;25:4813–4822. [PubMed: 15888657]
- Gan WB, Grutzendler J, Wong WT, Wong RO, Lichtman JW. Multicolor "DiOlistic" labeling of the nervous system using lipophilic dye combinations. *Neuron* 2000;27:219–225. [PubMed: 10985343]
- Gheorghita F, Kraftsik R, Dubois R, Welker E. Structural basis for map formation in the thalamocortical pathway of the barreless mouse. *J Neurosci* 2006;26:10057–10067. [PubMed: 17005869]
- Gil Z, Connors BW, Amitai Y. Efficacy of thalamocortical and intracortical synaptic connections: quanta, innervation, and reliability. *Neuron* 1999;23:385–397. [PubMed: 10399943]
- Golshani P, Hutnick L, Schweizer F, Fan G. Conditional Dnmt1 deletion in dorsal forebrain disrupts development of somatosensory barrel cortex and thalamocortical long-term potentiation. *Thalamus Relat Syst* 2005;3:227–233. [PubMed: 17710197]
- Groc L, Gustafsson B, Hanse E. AMPA signalling in nascent glutamatergic synapses: there and not there! *Trends Neurosci* 2006;29:132–139. [PubMed: 16443288]
- Gubellini P, Saulle E, Centonze D, Costa C, Tropepi D, Bernardi G, Conquet F, Calabresi P. Corticostriatal LTP requires combined mGluR1 and mGluR5 activation. *Neuropharmacology* 2003;44:8–16. [PubMed: 12559117]
- Guo W, Wei F, Zou S, Robbins MT, Sugiyo S, Ikeda T, Tu JC, Worley PF, Dubner R, Ren K. Group I metabotropic glutamate receptor NMDA receptor coupling and signaling cascade mediate spinal dorsal horn NMDA receptor 2B tyrosine phosphorylation associated with inflammatory hyperalgesia. *J Neurosci* 2004;24:9161–9173. [PubMed: 15483135]
- Hall BJ, Ghosh A. Regulation of AMPA receptor recruitment at developing synapses. *Trends Neurosci* 2008;31:82–89. [PubMed: 18201773]
- Hannan AJ, Blakemore C, Katsnelson A, Vitalis T, Huber KM, Bear M, Roder J, Kim D, Shin HS, Kind PC. PLC-beta1, activated via mGluRs, mediates activity-dependent differentiation in cerebral cortex. *Nat Neurosci* 2001;4:282–288. [PubMed: 11224545]
- Harney SC, Rowan M, Anwyl R. Long-term depression of NMDA receptor-mediated synaptic transmission is dependent on activation of metabotropic glutamate receptors and is altered to long-term potentiation by low intracellular calcium buffering. *J Neurosci* 2006;26:1128–1132. [PubMed: 16436598]
- Heidinger V, Manzerra P, Wang XQ, Strasser U, Yu SP, Choi DW, Behrens MM. Metabotropic glutamate receptor 1-induced upregulation of NMDA receptor current: mediation through the Pyk2/Src-family kinase pathway in cortical neurons. *J Neurosci* 2002;22:5452–5461. [PubMed: 12097497]
- Hensch TK. Critical period plasticity in local cortical circuits. *Nat Rev Neurosci* 2005;6:877–888. [PubMed: 16261181]
- Hessler NA, Shirke AM, Malinow R. The probability of transmitter release at a mammalian central synapse. *Nature* 1993;366:569–572. [PubMed: 7902955]
- Holcman D, Korkotian E, Segal M. Calcium dynamics in dendritic spines, modeling and experiments. *Cell Calcium* 2005;37:467–475. [PubMed: 15820395]
- Huber KM, Roder JC, Bear MF. Chemical induction of mGluR5- and protein synthesis--dependent long-term depression in hippocampal area CA1. *J Neurophysiol* 2001;86:321–325. [PubMed: 11431513]
- Hur EE, Zaborszky L. Vglut2 afferents to the medial prefrontal and primary somatosensory cortices: a combined retrograde tracing in situ hybridization. *J Comp Neurol* 2005;483:351–373. [PubMed: 15682395]
- Husi H, Ward MA, Choudhary JS, Blackstock WP, Grant SG. Proteomic analysis of NMDA receptor-adhesion protein signaling complexes. *Nat Neurosci* 2000;3:661–669. [PubMed: 10862698]
- Inan M, Crair MC. Development of cortical maps: perspectives from the barrel cortex. *Neuroscientist* 2007;13:49–61. [PubMed: 17229975]
- Inan M, Lu HC, Albright MJ, She WC, Crair MC. Barrel map development relies on protein kinase A regulatory subunit II beta-mediated cAMP signaling. *J Neurosci* 2006;26:4338–4349. [PubMed: 16624954]

- Ince-Dunn G, Hall BJ, Hu SC, Ripley B, Hugarir RL, Olson JM, Tapscott SJ, Ghosh A. Regulation of thalamocortical patterning and synaptic maturation by NeuroD2. *Neuron* 2006;49:683–695. [PubMed: 16504944]
- Isaac JT, Crair MC, Nicoll RA, Malenka RC. Silent synapses during development of thalamocortical inputs. *Neuron* 1997;18:269–280. [PubMed: 9052797]
- Isaac JT, Nicoll RA, Malenka RC. Evidence for silent synapses: implications for the expression of LTP. *Neuron* 1995;15:427–434. [PubMed: 7646894]
- Iwasato T, Datwani A, Wolf AM, Nishiyama H, Taguchi Y, Tonegawa S, Knopfel T, Erzurumlu RS, Itohara S. Cortex-restricted disruption of NMDAR1 impairs neuronal patterns in the barrel cortex. *Nature* 2000;406:726–731. [PubMed: 10963597]
- Iwasato T, Inan M, Kanki H, Erzurumlu RS, Itohara S, Crair MC. Cortical adenylyl cyclase 1 is required for thalamocortical synapse maturation and aspects of layer IV barrel development. *J Neurosci* 2008;28:5931–5943. [PubMed: 18524897]
- Jia Z, Lu Y, Henderson J, Taverna F, Romano C, Abramow-Newerly W, Wojtowicz JM, Roder J. Selective abolition of the NMDA component of long-term potentiation in mice lacking mGluR5. *Learn Mem* 1998;5:331–343. [PubMed: 10454358]
- Kenny PJ, Markou A. The ups and downs of addiction: role of metabotropic glutamate receptors. *Trends Pharmacol Sci* 2004;25:265–272. [PubMed: 15120493]
- Kidd FL, Isaac JT. Developmental and activity-dependent regulation of kainate receptors at thalamocortical synapses. *Nature* 1999;400:569–573. [PubMed: 10448859]
- Killackey HP, Leshin S. The organization of specific thalamocortical projections to the posteromedial barrel subfield of the rat somatic sensory cortex. *Brain Res* 1975;86:469–472. [PubMed: 1116010]
- Kim CH, Lee J, Lee JY, Roche KW. Metabotropic glutamate receptors: Phosphorylation and receptor signaling. *J Neurosci Res* 2007;86:1–10. [PubMed: 17663464]
- Lopez-Bendito G, Shigemoto R, Fairen A, Lujan R. Differential distribution of group I metabotropic glutamate receptors during rat cortical development. *Cereb Cortex* 2002;12:625–638. [PubMed: 12003862]
- Lu HC, Butts DA, Kaeser PS, She WC, Janz R, Crair MC. Role of efficient neurotransmitter release in barrel map development. *J Neurosci* 2006;26:2692–2703. [PubMed: 16525048]
- Lu HC, Gonzalez E, Crair MC. Barrel cortex critical period plasticity is independent of changes in NMDA receptor subunit composition. *Neuron* 2001;32:619–634. [PubMed: 11719203]
- Lu HC, She WC, Plas DT, Neumann PE, Janz R, Crair MC. Adenylyl cyclase I regulates AMPA receptor trafficking during mouse cortical 'barrel' map development. *Nat Neurosci* 2003;6:939–947. [PubMed: 12897788]
- Lu YM, Jia Z, Janus C, Henderson JT, Gerlai R, Wojtowicz JM, Roder JC. Mice lacking metabotropic glutamate receptor 5 show impaired learning and reduced CA1 long-term potentiation (LTP) but normal CA3 LTP. *J Neurosci* 1997;17:5196–5205. [PubMed: 9185557]
- Lubke J, Egger V, Sakmann B, Feldmeyer D. Columnar organization of dendrites and axons of single and synaptically coupled excitatory spiny neurons in layer 4 of the rat barrel cortex. *J Neurosci* 2000;20:5300–5311. [PubMed: 10884314]
- Malinow R, Malenka RC. AMPA receptor trafficking and synaptic plasticity. *Annu Rev Neurosci* 2002;25:103–126. [PubMed: 12052905]
- Manabe T, Nicoll RA. Long-term potentiation: evidence against an increase in transmitter release probability in the CA1 region of the hippocampus. *Science* 1994;265:1888–1892. [PubMed: 7916483]
- Munoz A, Liu XB, Jones EG. Development of metabotropic glutamate receptors from trigeminal nuclei to barrel cortex in postnatal mouse. *J Comp Neurol* 1999;409:549–566. [PubMed: 10376739]
- Nahmani M, Erisir A. VGluT2 immunocytochemistry identifies thalamocortical terminals in layer 4 of adult and developing visual cortex. *J Comp Neurol* 2005;484:458–473. [PubMed: 15770654]
- Nevian T, Sakmann B. Spine Ca<sup>2+</sup> signaling in spike-timing-dependent plasticity. *J Neurosci* 2006;26:11001–11013. [PubMed: 17065442]
- Neyman S, Manahan-Vaughan D. Metabotropic glutamate receptor 1 (mGluR1) and 5 (mGluR5) regulate late phases of LTP and LTD in the hippocampal CA1 region in vitro. *Eur J Neurosci* 2008;27:1345–1352. [PubMed: 18364018]

- Petersen RS, Diamond ME. Spatial-temporal distribution of whisker-evoked activity in rat somatosensory cortex and the coding of stimulus location. *J Neurosci* 2000;20:6135–6143. [PubMed: 10934263]
- Puyal J, Grassi S, Dieni C, Frondaroli A, Dememes D, Raymond J, Pettorossi VE. Developmental shift from long-term depression to long-term potentiation in the rat medial vestibular nuclei: role of group I metabotropic glutamate receptors. *J Physiol* 2003;553:427–443. [PubMed: 12972627]
- Quairiaux C, Armstrong-James M, Welker E. Modified sensory processing in the barrel cortex of the adult mouse after chronic whisker stimulation. *J Neurophysiol* 2007;97:2130–2147. [PubMed: 17122325]
- Rebsam A, Seif I, Gaspar P. Refinement of thalamocortical arbors and emergence of barrel domains in the primary somatosensory cortex: a study of normal and monoamine oxidase a knock-out mice. *J Neurosci* 2002;22:8541–8552. [PubMed: 12351728]
- Rosenmund C, Clements JD, Westbrook GL. Nonuniform probability of glutamate release at a hippocampal synapse. *Science* 1993;262:754–757. [PubMed: 7901909]
- Shi J, Townsend M, Constantine-Paton M. Activity-dependent induction of tonic calcineurin activity mediates a rapid developmental downregulation of NMDA receptor currents. *Neuron* 2000;28:103–114. [PubMed: 11086987]
- Simons DJ, Woolsey TA. Functional organization in mouse barrel cortex. *Brain Res* 1979;165:327–332. [PubMed: 421142]
- Song I, Huganir RL. Regulation of AMPA receptors during synaptic plasticity. *Trends Neurosci* 2002;25:578–588. [PubMed: 12392933]
- Steffen H, Van der Loos H. Early lesions of mouse vibrissal follicles: their influence on dendrite orientation in the cortical barrelfield. *Exp Brain Res* 1980;40:419–431. [PubMed: 7439284]
- Sung KW, Choi S, Lovinger DM. Activation of group I mGluRs is necessary for induction of long-term depression at striatal synapses. *J Neurophysiol* 2001;86:2405–2412. [PubMed: 11698530]
- Takasaki C, Okada R, Mitani A, Fukaya M, Yamasaki M, Fujihara Y, Shirakawa T, Tanaka K, Watanabe M. Glutamate transporters regulate lesion-induced plasticity in the developing somatosensory cortex. *J Neurosci* 2008;28:4995–5006. [PubMed: 18463253]
- Van der Loos H, Welker E, Dorfl J, Rumo G. Selective breeding for variations in patterns of mystacial vibrissae of mice. Bilaterally symmetrical strains derived from ICR stock. *J. Hered* 1986;77:66–82. [PubMed: 3711643]
- Vitalis T, Cases O, Gillies K, Hanoun N, Hamon M, Seif I, Gaspar P, Kind P, Price DJ. Interactions between TrkB signaling and serotonin excess in the developing murine somatosensory cortex: a role in tangential and radial organization of thalamocortical axons. *J Neurosci* 2002;22:4987–5000. [PubMed: 12077195]
- Watson RF, Abdel-Majid RM, Barnett MW, Willis BS, Katsnelson A, Gillingwater TH, McKnight GS, Kind PC, Neumann PE. Involvement of protein kinase A in patterning of the mouse somatosensory cortex. *J Neurosci* 2006;26:5393–5401. [PubMed: 16707791]
- Welker C. Receptive fields of barrels in the somatosensory neocortex of the rat. *J Comp Neurol* 1976;166:173–189. [PubMed: 770516]
- Welker E, Armstrong-James M, Bronchti G, Qurednik W, Gheorghita-Baechler F, Dubois R, Guernsey DL, Van der Loos H, Neumann PE. Altered sensory processing in the somatosensory cortex of the mouse mutant barrelless. *Science* 1996;271:1864–1867. [PubMed: 8596955]
- Welker E, Armstrong-James M, Van der Loos H, Kraftsik R. The mode of activation of a barrel column: response properties of single units in the somatosensory cortex of the mouse upon whisker deflection. *Eur J Neurosci* 1993;5:691–712. [PubMed: 8261141]
- Welker E, Van der Loos H. Is areal extent in sensory cerebral cortex determined by peripheral innervation density? *Exp Brain Res* 1986a;63:650–654. [PubMed: 3758273]
- Welker E, Van der Loos H. Quantitative correlation between barrel-field size and the sensory innervation of the whiskerpad: a comparative study in six strains of mice bred for different patterns of mystacial vibrissae. *J Neurosci* 1986b;6:3355–3373. [PubMed: 3772437]
- Wijetunge LS, Till SM, Gillingwater TH, Ingham CA, Kind PC. mGluR5 regulates glutamate-dependent development of the mouse somatosensory cortex. *J Neurosci* 2008;28:13028–13037. [PubMed: 19052194]

- Woolsey TA, Dierker ML, Wann DF. Mouse SmI cortex: qualitative and quantitative classification of golgi-impregnated barrel neurons. *Proc Natl Acad Sci U S A* 1975;72:2165–2169. [PubMed: 1056021]
- Woolsey TA, Van der Loos H. The structural organization of layer IV in the somatosensory region (SI) of the mouse cerebral cortex. *Brain Res* 1970;17:205–242. [PubMed: 4904874]
- Xu-Friedman MA, Regehr WG. Presynaptic strontium dynamics and synaptic transmission. *Biophys J* 1999;76:2029–2042. [PubMed: 10096899]
- Yanagisawa T, Tsumoto T, Kimura F. Transiently higher release probability during critical period at thalamocortical synapses in the mouse barrel cortex: relevance to differential short-term plasticity of AMPA and NMDA EPSCs and possible involvement of silent synapses. *Eur J Neurosci* 2004;20:3006–3018. [PubMed: 15579155]
- Zucker RS, Regehr WG. Short-term synaptic plasticity. *Annu Rev Physiol* 2002;64:355–405. [PubMed: 11826273]

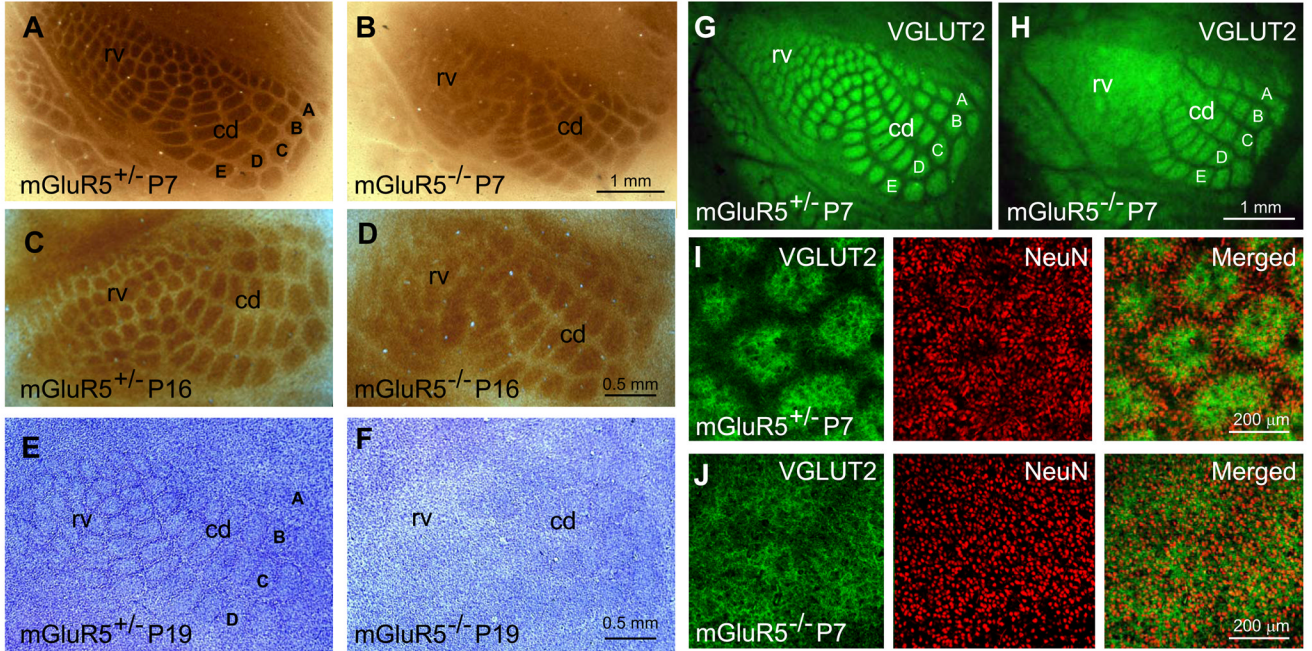


**Figure 1. Whisker maps are abnormal in mGluR5<sup>-/-</sup> S1 cortex**  
 (A–D) Sample images of CO-stained tangential sections through cortical layer IV prepared from P7 (A,B), and P16 (C,D) of mGluR5<sup>+/+</sup> (A,C) and mGluR5<sup>-/-</sup> (B,D,) S1 cortex. (E,F) Distinct barrel walls revealed by Nissl staining were seen in mGluR5<sup>+/+</sup> (E), but not in mGluR5<sup>-/-</sup> S1 cortex (F). (G–J) VGLuT2-immunoreactivity in tangential sections revealed the distribution of TCAs in P7 mGluR5<sup>+/+</sup> mice (G,I) and mGluR5<sup>-/-</sup> mice (H,J). (G–H) Representative images of VGLuT2 and NeuN double-labeling show that the organizations of TCAs and cortical neurons (labeled by NeuN antibody) were both disrupted in the representation of the rostro-ventral whiskers (rv) of mGluR5<sup>-/-</sup> mice. All the mGluR5<sup>+/+</sup> mice represent paired littermate controls and staining was performed simultaneously. Abbreviations: A–E indicates the representation for A–E rows whiskers; rv, the representation of the rostro-ventral whiskers; cd, that of the caudo-rostral whiskers.

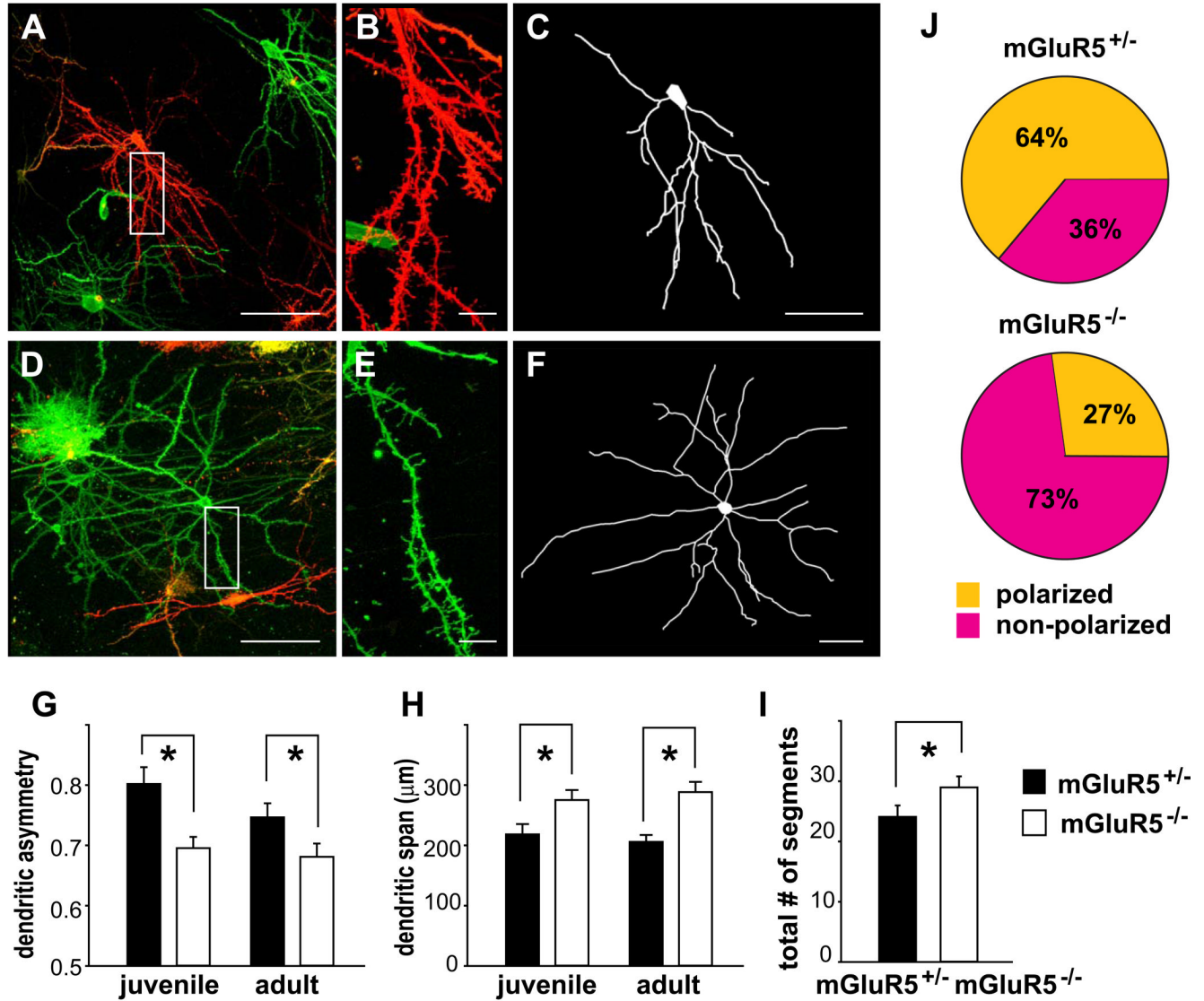


**Figure 2. mGluR5 is required for full polarization of layer IV spiny stellate neurons** (A–F) Low magnification images show “DiOlistic” labeled layer IV mGluR5<sup>+/+</sup> (A) and mGluR5<sup>-/-</sup> (D) spiny stellate neurons. Enlarged views show the dendritic spines (B,E). C and F show their computer-aided reconstructions. (G) The degree of dendritic asymmetry is significantly lower in mGluR5<sup>-/-</sup> neurons from both juvenile ( $p = 0.003$ ) and adult groups ( $p = 0.048$ ). (H) The dendritic span is significantly broader in mGluR5<sup>-/-</sup> neurons from both juvenile ( $p = 0.018$ , Mann-Whitney *U* Test) and adult animals ( $p < 0.001$ ). (I) The total number of dendritic segments is significantly higher in mGluR5<sup>-/-</sup> neurons ( $p = 0.048$ , Mann-Whitney *U* Test). (J) Pie charts showing the percentage of cells with polarized or non-polarized distributions of dendrites (neurons with a dendritic asymmetry value greater than 0.75 were considered to be polarized). Scale bars: 100 µm for A,D; 10 µm for B,E; 50 µm for C,F. Asterisks indicate significant differences.

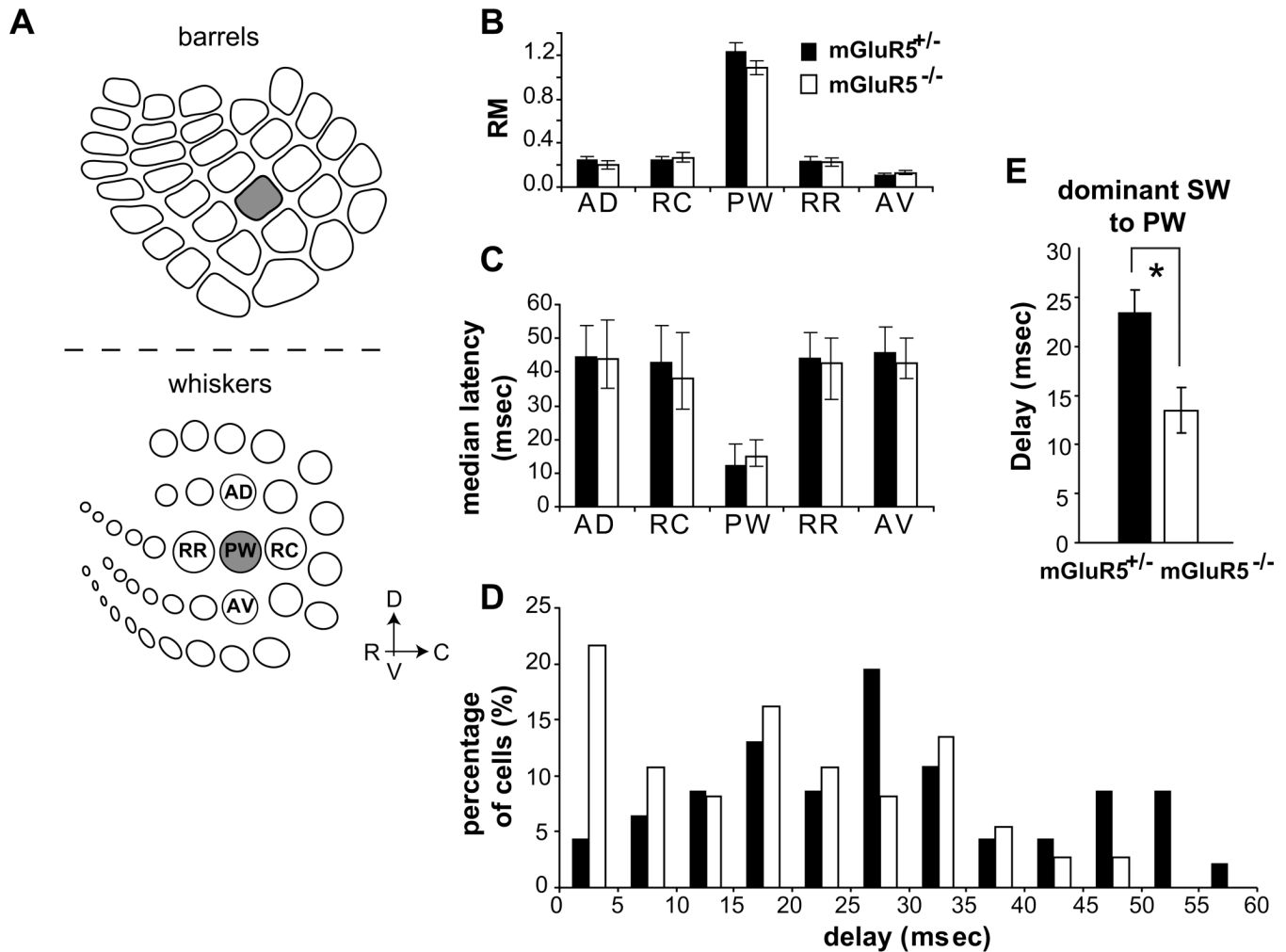


**Figure 3. Normal topographical representations for individual whiskers were detected in mGluR5<sup>-/-</sup> mice with single unit recordings**

(A) Extracellular single unit responses evoked by whisker deflections were acquired from layer IV neurons located in C1, C2 and D2 barrels. Evoked activity was recorded in response to the principal whisker (PW) and to immediate surround whiskers (SWs): AD, the whisker dorsal to the PW and on the same arc; AV, the whisker ventral to the PW and on the same arc; C, caudal; D, dorsal; R, rostral; RC, the whisker rostral to the PW and on the same row; RR, the whisker caudal to the PW and on the same row; V, ventral. (B) There was a slight but insignificant decrease in the RM to PW deflections in mGluR5<sup>-/-</sup> mice ( $p = 0.15$ ). (C) Short latency responses were triggered by PW in both genotypes (plotted with median and interquartile ranges; mGluR5<sup>+/-</sup>, median is 12.5 ms; mGluR5<sup>-/-</sup>, median is 15 ms;  $p = 0.71$ ). (D) The distribution of the latency differences (delays) between responses to the PW and the dominant SW was altered in the mGluR5<sup>-/-</sup> mice. In mGluR5<sup>+/-</sup> mice, only 4% of neurons show a latency delay  $\leq 5$  ms. However, in the mGluR5<sup>-/-</sup> mice, the proportion of neurons responding to the dominant SW with a delay  $\leq 5$  ms increased to more than 20%. (E) The delay is significantly shorter in the mGluR5<sup>-/-</sup> mice than in the mGluR5<sup>+/-</sup> mice (asterisk;  $p = 0.005$ , non-parametric Mann-Whitney U test).

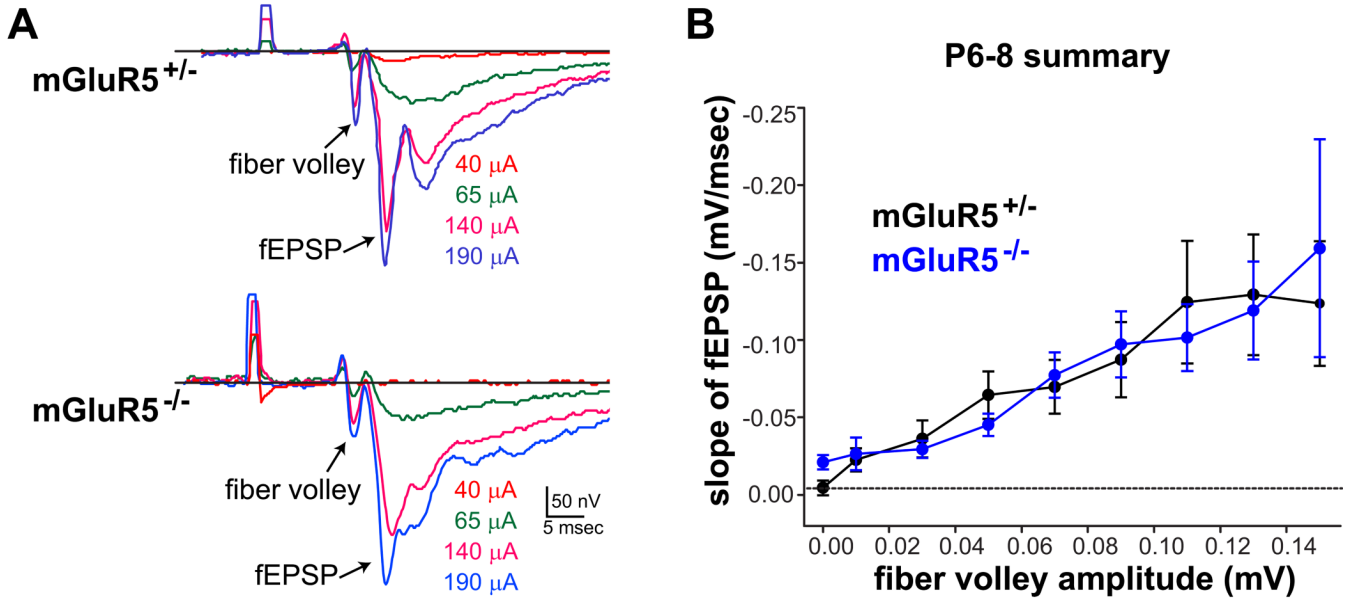


**Figure 4. Normal input-output relationship in mGluR5<sup>-/-</sup> TC synapses**

(A) Representative traces of field potential responses (average of ten sweeps) evoked by different stimulus strength (individual traces are color coded with the strength indicated on the right side) in mGluR5<sup>+/-</sup> and mGluR5<sup>-/-</sup> TC pathways. Both the amplitudes of the fiber volley and the slopes of the fEPSP increased as the stimulation strength were increased. (B) Summary of the input-output relationships for mGluR5<sup>+/-</sup> (black, n = 6) and mGluR5<sup>-/-</sup> TC synapses (grey, n = 8). Both response curves are linear and extensively overlap with each other.

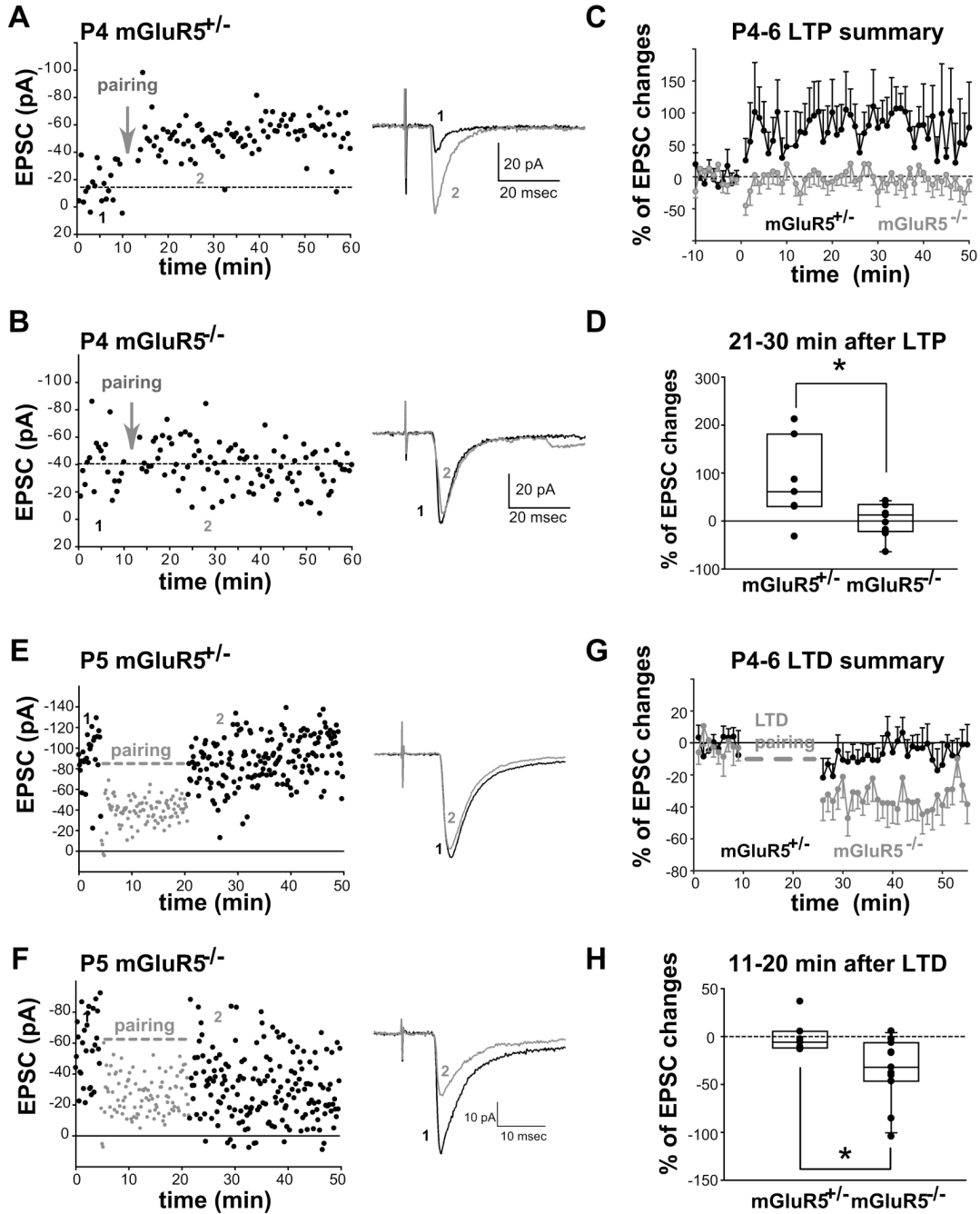


**Figure 5. LTP is absent while LTD is enhanced in mGluR5<sup>-/-</sup> TC synapses**

(A,B) Representative whole-cell voltage clamp recordings from P4 mGluR5<sup>+/-</sup> and mGluR5<sup>-/-</sup> neurons. The thalamocortical responses in mGluR5<sup>+/-</sup> (A) but not in mGluR5<sup>-/-</sup> (B) layer IV neurons were potentiated after an LTP pairing paradigm (indicated by arrows; 100 Hz stimuli, concurrently depolarizing the cell to -10 mV). Sample traces (average of 20 sweeps) before (1) and after (2) the LTP pairing paradigm are shown to the right (A,B). (C) Summary of LTP pairing experiments from P4-6 mice. (D) Summary of EPSC % changes 21-30 minutes after pairing with each dot representing an individual recording (p = 0.026). (E,F) Representative examples of LTD induction at TC synapses from a P5 mGluR5<sup>+/-</sup> (E) and a P5 mGluR5<sup>-/-</sup> neuron (F). Traces (average of 20 sweeps) before (1) and after (2) the

LTD pairing paradigm are shown on the right. Substantial and long-lasting depression of EPSCs was triggered by the LTD pairing paradigm (100 0.1 Hz stimuli, concurrently depolarizing the cell to  $-40$  mV) in an mGluR5<sup>-/-</sup> neuron (**F**) while a relatively small depression was induced by the same pairing paradigm in an mGluR5<sup>+/-</sup> neuron (**E**). (**G**) Summary graph of LTD pairing experiments from P4–6 mice. Significant LTD was induced in mGluR5<sup>-/-</sup> TC synapses. (**H**) Summary of EPSC % changes 11–20 minutes after pairing with each dot representing an individual recording ( $p = 0.03$ , Mann-Whitney  $U$  test). Note that this pairing protocol occasionally induced potentiation of thalamocortical responses (two mGluR5<sup>+/-</sup> and one mGluR5<sup>-/-</sup> neurons). Asterisk indicates a significant difference.

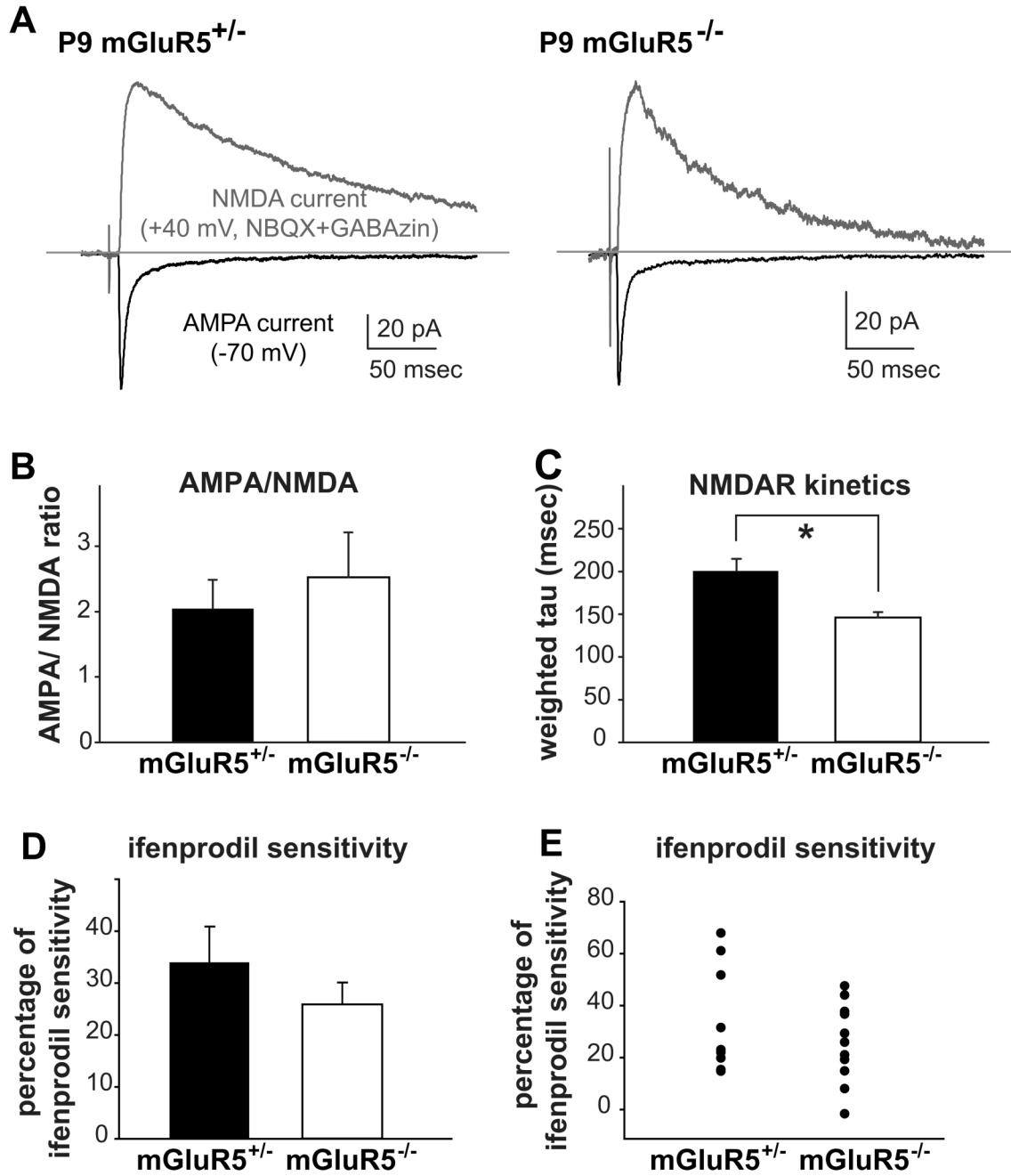


**Figure 6. NMDA current kinetics are faster at TC synapses in mGluR5<sup>-/-</sup> mice**  
 (A) Representative traces of AMPA and NMDA currents (average of ten sweeps) recorded from P9 mGluR5<sup>+/-</sup> and mGluR5<sup>-/-</sup> TC synapses. (B) Summary of AMPA/NMDA current ratios ( $p = 0.165$ , Mann-Whitney  $U$  Test). (C) The weighted time constants ( $\tau$ ) for NMDA currents from layer IV neurons in mGluR5<sup>-/-</sup> mice are significantly faster than from mGluR5<sup>+/-</sup> mice ( $p=0.008$ ). (D,E) In mGluR5<sup>-/-</sup> mice, there is a small but statistically insignificant decrease in ifenprodil sensitivity ( $p = 0.303$ ; asterisk). The summaries of the percentage of ifenprodil sensitivity are presented as bar graphs (D) and scatter plots (E) with each dot representing an individual recording.

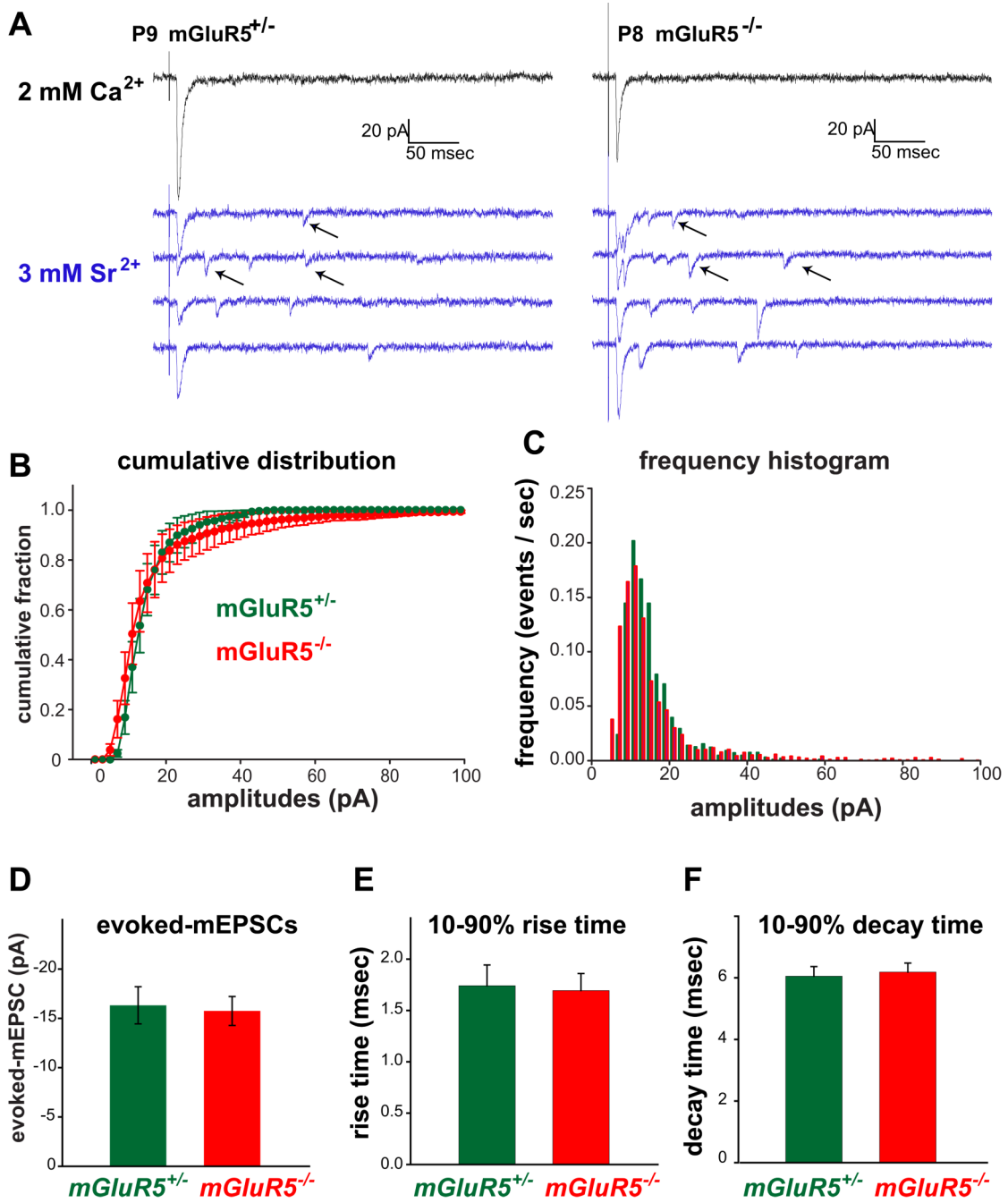


**Figure 7. Evoked AMPA-mEPSCs are similar at mGluR5<sup>+/-</sup> and mGluR5<sup>-/-</sup> TC synapses**  
 (A) Representative traces of evoked responses in 2 mM Ca<sup>2+</sup>- (black) and 3 mM Sr<sup>2+</sup>-ACSF (blue) from recordings in a P9 mGluR5<sup>+/-</sup> and a P8 mGluR5<sup>-/-</sup> neurons. The substitution of Ca<sup>2+</sup> with Sr<sup>2+</sup> quickly led to a reduction in the amplitudes of synchronized EPSCs and the appearance of numerous asynchronous quantal events (indicated by arrows). The amplitudes of quantal events in Sr<sup>2+</sup>-ACSF reflects the response to the release of single vesicle. (B) Summary of the normalized average cumulative amplitude histograms for mGluR5<sup>+/-</sup> (green) and mGluR5<sup>-/-</sup> mice (red). (C) The frequency histogram of the amplitudes. (D-F) No difference was found in the average amplitudes (D), 10–90% rise time (E), and 10–90% decay time (F) of evoked-mEPSCs between mGluR5<sup>+/-</sup> (green) and mGluR5<sup>-/-</sup> mice (red).

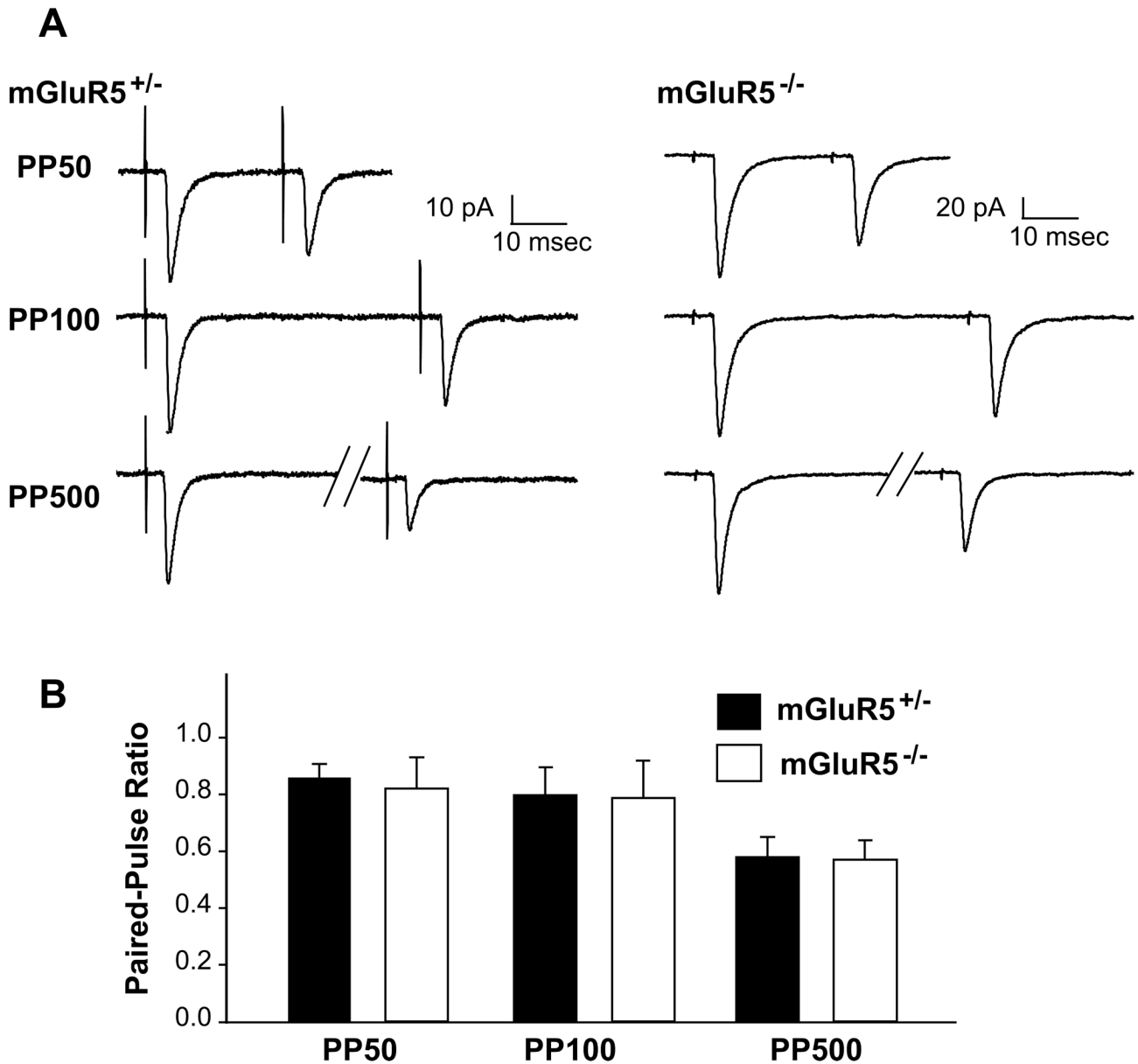


**Figure 8. Normal short-term plasticity at mGluR5<sup>-/-</sup> TC synapses**

(A) Example traces (average of ten sweeps) of AMPAR-mediated TC responses triggered by a paired stimuli with 50, 100, 500 msec inter-stimulus intervals (PP50, PP100, PP500). Strong paired-pulse depression was evoked in P8 mGluR5<sup>+/-</sup> and mGluR5<sup>-/-</sup> cells. (B) Summary of P7–9 AMPA-PP ratios. No difference was found between mGluR5<sup>+/-</sup> and mGluR5<sup>-/-</sup> PP ratios.

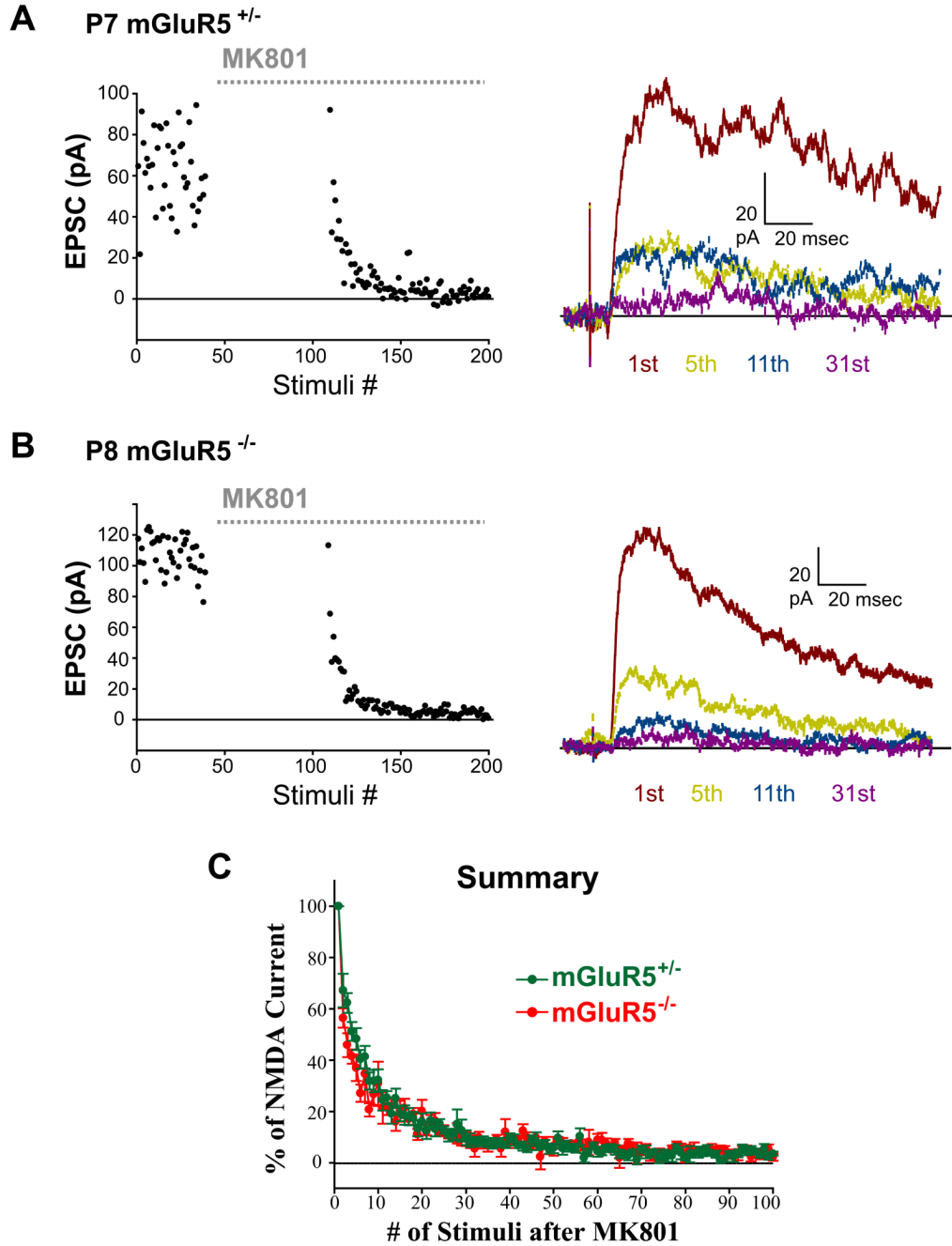


**Figure 9. mGluR5<sup>-/-</sup> TCAs have normal release probability**  
 (A,B) Representative examples of MK801 experiments in single mGluR5<sup>+/-</sup> (A) and mGluR5<sup>-/-</sup> (B) cells showing the progressive block of NMDA-EPSCs by 40  $\mu$ M MK801. Amplitude distributions of NMDA-EPSCs during MK801 treatment are illustrated on the left. On the right, the first, 5<sup>th</sup>, 11<sup>th</sup> and 31<sup>st</sup> traces after stimulation resumes in the presence of MK801 are shown on the right. (C) Summary graph of MK801 experiments for P6-P8 mGluR5<sup>+/-</sup> and mGluR5<sup>-/-</sup> cells. All the values are normalized in each experiment to the amplitude of the first EPSC evoked in the presence of MK801 and averaged for each mouse group. The amplitudes of NMDA-EPSCs decreased very rapidly in both genotypes. By the fifth stimulus, more than 60% of the EPSC was inhibited by MK801.